Check for updates

Geochemistry, Geophysics, Geosystems®

AGU ADVANCING EARTH AND SPACE SCIENCES

RESEARCH ARTICLE
10.1029/2026GC013203

Key Points:

- Newfoundland margin peridotites preserve records of pre-rifting evolution despite pervasive serpentinization
- The depleted character of Newfoundland margin peridotites reflects high degrees of melt extraction prior to Triassic rifting
- Long-term evolution of the lithospheric mantle and mantle inheritance significantly influence continental break up and associated magmatism

Supporting Information:

Supporting Information may be found in the online version of this article.

Correspondence to:

A. Secchiari,
arianna.secchiari@unimi.it

Citation:

Secchiari, A., Godard, M., & Montanini, A. (2026). Multistage evolution and inheritance in a magma-poor conjugate margin: Insights from serpentinized peridotites of the Newfoundland margin (ODP Hole 1277A). *Geochemistry, Geophysics, Geosystems*, *27*, e2026GC013203. https://doi.org/10.1029/2026GC013203

Received 28 MAY 2026
Accepted 11 SEP 2026

Author Contributions:

Conceptualization: A. Secchiari, M. Godard, A. Montanini
Data curation: A. Secchiari
Formal analysis: A. Secchiari
Funding acquisition: A. Secchiari
Investigation: A. Secchiari
Methodology: A. Secchiari, M. Godard, A. Montanini
Project administration: A. Secchiari
Validation: A. Secchiari, M. Godard, A. Montanini
Writing – original draft: A. Secchiari

© 2026 The Author(s). Geochemistry, Geophysics, Geosystems published by Wiley Periodicals LLC on behalf of American Geophysical Union.
This is an open access article under the terms of the Creative Commons Attribution License, which permits use, distribution and reproduction in any medium, provided the original work is properly cited.

Multistage Evolution and Inheritance in a Magma-Poor Conjugate Margin: Insights From Serpentinized Peridotites of the Newfoundland Margin (ODP Hole 1277A)

A. Secchiari[1], M. Godard[2], and A. Montanini[3]

[1]Earth Sciences Department "A.Desio", University of Milan, Milan, Italy, [2]Géosciences Montpellier, CNRS, University of Montpellier, Montpellier, France, [3]Department of Chemistry, Life Sciences and Environmental Sustainability, University of Parma, Parma, Italy

Abstract The nature of mantle sections exhumed at magma-poor rifted margins remains poorly constrained, largely because direct sampling of mantle in modern passive margins is exceptionally rare. The Iberia–Newfoundland system is unique in providing drilled mantle rocks on both conjugate margins, offering an unprecedented glimpse into mantle heterogeneity across an entire rift system. Here we present new in situ major and trace element data from highly serpentinized peridotites recovered at ODP Hole 1277A (Newfoundland margin). The samples display mylonitic textures and are strongly depleted in clinopyroxene (≤2 vol.%). Despite pervasive serpentinization, relict mantle minerals retain evidence of high melt extraction degrees, as indicated by Al_2O_3-poor orthopyroxene (2.36–3.19 wt.%) and orthopyroxene trace element systematics. Geochemical modeling of orthopyroxene REE compositions indicates ≥14% melt extraction initiated in the garnet stability field, likely predating the Jurassic rifting. Following depletion, the mantle was locally overprinted by melt-rock interaction, as highlighted by high and variable spinel Cr#, REE disequilibrium in coexisting pyroxenes, and clinopyroxene with atypical V-shaped REE profiles (La_N/Sm_N = 4.3). During Jurassic rifting, the Newfoundland margin mantle section was reactivated and deformed within lithospheric-scale shear zones, leading to mylonitization and exhumation. The refractory nature of the mantle likely promoted limited melt extraction and retention of these transient melts within the lithosphere, now preserved as spinel-pyroxene symplectites. Subsequent cooling enabled hydration at ~500–600°C and ultimately pervasive serpentinization. These results highlight that the pre-rift evolution of the lithospheric mantle exerts a primary control on the evolution of magma-poor rifted margins.

Plain Language Summary When continental rifting leads to the formation of new oceans, mantle rocks can be brought closer to the surface and accessed through scientific drilling. In settings where magmatism is limited, the so-called "magma-poor" margins, these rocks may preserve a record of geological processes that predate rifting itself. In this study, we investigated peridotites drilled offshore Newfoundland at ODP Site 1277. Although these rocks are now strongly altered by seawater (a process known as serpentinization), we show that they still retain signatures of their earlier mantle history. Our results indicate that this mantle section first underwent partial melting at a great depth, acquiring a refractory character. Later, it was locally modified through interaction with small amounts of enriched melts. During continental breakup, this refractory mantle was exhumed along large-scale shear zones, resulting in mylonitic deformation, possibly favored by the presence of low-volume melt fractions. By comparing Newfoundland with the conjugate margin of West Iberia, we demonstrate that continental break up and associated magmatism are significantly influenced by long-term evolution of the lithospheric mantle.

1. Introduction

Magma-poor rifted margins provide a unique window into lithospheric thinning, mantle exhumation, and the transition to seafloor spreading following rifting initiation and lithospheric break up. The Iberia–Newfoundland system is unique: it is the only conjugate margin where mantle has been directly sampled by deep ocean drilling on both sides (Boillot et al., 1987; Tucholke & Sibuet, 2007; Whitmarsh & Sawyer, 1996). It offers an exceptional opportunity to investigate the evolution of subcontinental lithospheric mantle (SCLM), from incipient extension to break up, at a magma-poor Ocean Continent Transition (OCT).

Writing – review & editing: A. Secchiari, M. Godard, A. Montanini

On the West Iberian margin (WIM), mantle rocks display pronounced heterogeneity, ranging from refractory spinel harzburgites to refertilized plagioclase-bearing peridotites, and record a complex interplay of melt depletion, melt–rock interaction, and metasomatic overprints before and during rifting (e.g., Abe, 2001; Chazot et al., 2005; Hébert et al., 2001; Secchiari et al., 2025). By contrast, the Newfoundland margin (NFM) mantle is less well known. It was drilled only at ODP Site 1277 (Figure 1a), where refractory spinel harzburgites were recovered.

Their mineral compositions were interpreted as residues of 14%–25% partial melting in the spinel stability field, possibly linked to an ancient subduction-modified mantle reactivated during rifting (Müntener & Manatschal, 2006). Although systematically more refractory than the WIM peridotites, the NFM peridotites are affected by extreme serpentinization (>85%–90%), making their comprehensive petrological and geochemical investigation particularly challenging.

In this study, we revisit the NFM peridotites as a key archive of mantle evolution along the Iberia-Newfoundland conjugate margin. To minimize the effects of serpentinization, we exclusively focus on in situ mineral-scale characterization. We present the first comprehensive data set for peridotites from ODP Hole 1277A, including major and trace-element compositions of primary mantle minerals. This approach provides new insights into mantle evolution along the magma-poor rifted margin. Specifically, we address three key questions: (a) To what extent do highly serpentinized NFM peridotites preserve records of their pre-serpentinization mantle history? (b) Do these peridotites record inherited subcontinental lithospheric mantle (SCLM) signatures or evidence of supra-subduction zone (SSZ) processes? (c) What can be learned about the nature of mantle exhumed at modern magma-poor rifted margins from the Newfoundland–Iberia comparison?

By combining major and trace element compositions of the NFM peridotites, we will show that these rock-types retain a robust record of primary mantle evolution, despite pervasive serpentinization. This highlights their value as reliable tracers of mantle processes at magma-poor rifted margins and underscores the preservation of mineral signatures in highly serpentinized peridotite sections.

2. Geological Setting and Site Characteristics

The Iberia-Newfoundland conjugate margins represent a classic example of a magma-poor passive rift system, formed through a multiphase rifting evolution spanning from the Late Triassic to the Early Cretaceous. This prolonged extensional phase culminated in the opening of the North Atlantic and the separation of the North American (Flemish Cap) and European (Iberian) plates (Figure 1b). One of the most distinguishing features of this margin system is the limited production of syn-rift magmas (Beard et al., 2002; Cornen et al., 1996; Seifert et al., 1997), despite extreme lithospheric thinning (Lymer & Reston, 2022).

Rifting proceeded through two main stages. The initial phase, beginning in the Late Triassic and extending to the Early Jurassic, was characterized by the development of a fault-bounded intracontinental basin associated with moderate crustal stretching. The second, active from the Late Jurassic to the Early Cretaceous, involved extreme crustal thinning and culminated in the tectonic exhumation of subcontinental lithospheric mantle. This led to the formation of an extensive OCT zone, which locally exceeded 170 km in width (Péron-Pinvidic & Manatschal, 2009; Péron-Pinvidic et al., 2007).

Seismic and geological data from the Newfoundland margin reveal a well-developed tripartite crustal architecture across the OCT, comprising: (a) severely thinned continental crust; (b) a peridotite basement, composed of exhumed serpentinized mantle interlayered with remnants of thinned continental crust and minor intrusive bodies; (c) a proto-oceanic crust, heterogeneously composed of serpentinized peridotite and sparsely distributed gabbroic and basaltic units emplaced during the earliest stages of seafloor spreading (Shillington et al., 2006).

ODP Hole 1277A, situated atop the Mauzy Ridge, offers a critical window into the structure and composition of the peridotite basement in the Newfoundland margin (Figure S1 in Supporting Information S1). Drilling penetrated to 180.37 m below the seafloor (bsf) and recovered two main lithostratigraphic units. The upper ∼100 m comprise sedimentary rocks, underlain by a complex igneous–sedimentary succession (Unit 1). This unit consists of alternating basaltic flows, sandstones, and coarse breccias containing clasts of serpentinite and gabbro. The gabbroic rocks range from gabbros and gabbronorites to oxide gabbros and anorthosites. They are composed of clinopyroxene, plagioclase, ilmenite, Ti-pargasite and rare biotite and sulfides (Müntener & Manatschal, 2006).

15252027, 2026, 10, Downloaded from https://agupubs.onlinelibrary.wiley.com/doi/10.1029/2026GC013203 by CochraneItalia, Wiley Online Library on [07/10/2026]. See the Terms and Conditions (https://onlinelibrary.wiley.com/terms-and-conditions) on Wiley Online Library for rules of use; OA articles are governed by the applicable Creative Commons License

10.1029/2026GC013203

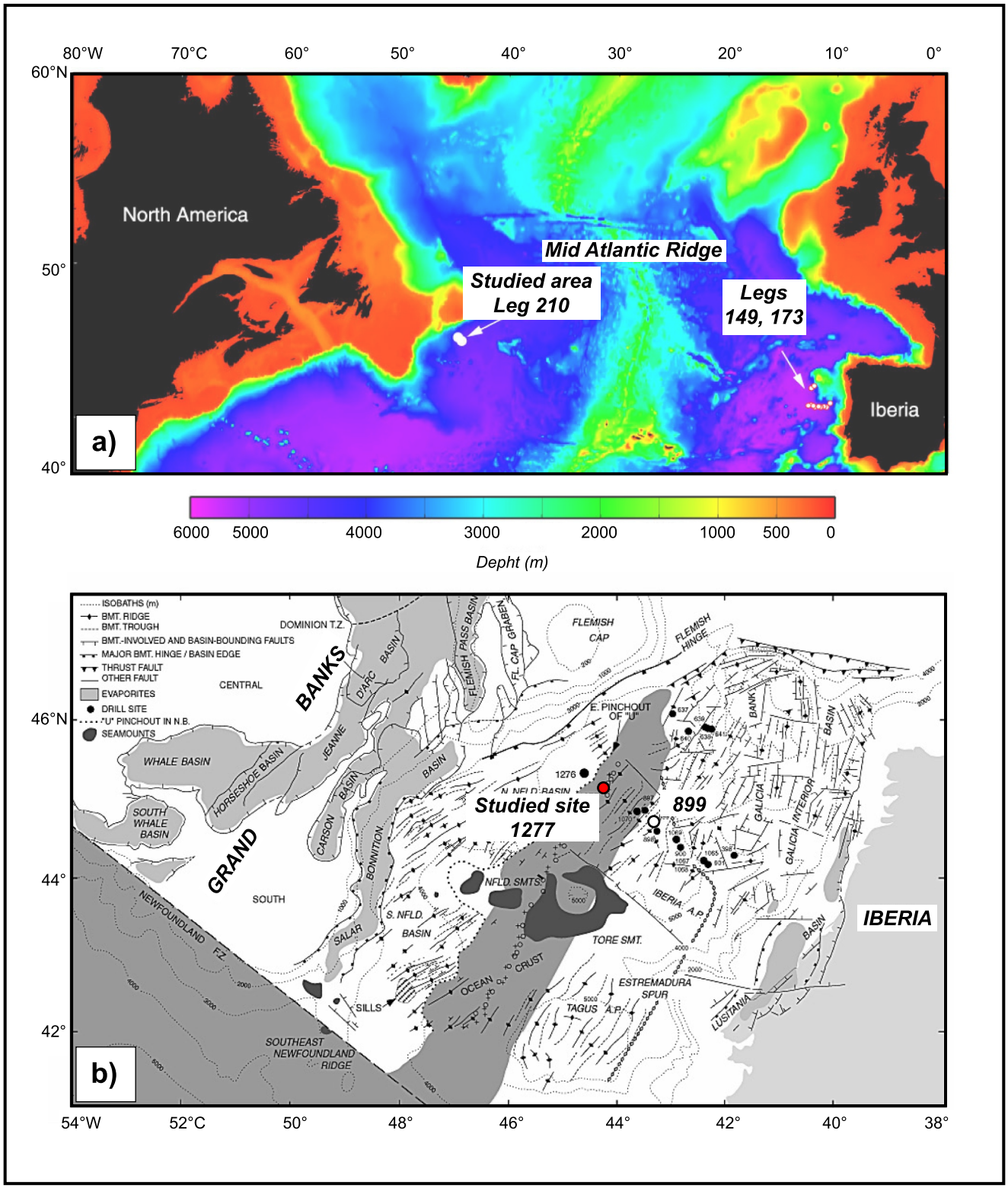


Figure 1. Sketch map of the Iberia-Newfoundland rift system showing the main drill sites along the conjugate margins. (a) Bathymetric map of the North Atlantic Ocean showing ODP/IODP sites from the Newfoundland Basin (Leg 210) and the western Iberia margin (Legs 149 and 173). (b) Tectonic reconstruction of the conjugate Newfoundland-Iberia margins showing Site 1277 in the Newfoundland Basin (solid circle) and Site 899 on the west Iberia margin (open circle).

15252027, 2026, 10, Downloaded from https://agupubs.onlinelibrary.wiley.com/doi/10.1029/2026GC013203 by CochraneItalia, Wiley Online Library on [07/10/2026]. See the Terms and Conditions (https://onlinelibrary.wiley.com/terms-and-conditions) on Wiley Online Library for rules of use; OA articles are governed by the applicable Creative Commons License

15252027, 2026, 10, Downloaded from https://agupubs.onlinelibrary.wiley.com/doi/10.1029/2026GC013203 by CochraneItalia, Wiley Online Library on [07/10/2026]. See the Terms and Conditions (https://onlinelibrary.wiley.com/terms-and-conditions) on Wiley Online Library for rules of use; OA articles are governed by the applicable Creative Commons License

Unit 1 unconformably overlies Unit 2, a serpentinized peridotite basement composed predominantly of spinel harzburgite, interlayered with matrix-supported breccias containing clasts ranging from undeformed serpentinite to mylonitic peridotite. The textural and structural diversity of these clasts is consistent with derivation from an underlying, variably deformed mantle basement (Müntener & Manatschal, 2006).

Previous petrological data indicate that Site 1277 harzburgites are extremely refractory, with Cr-rich spinel compositions reflecting 14%–25% degrees of partial melting in the spinel stability field. Müntener and Manatschal (2006) interpreted these rocks as fragments of an ancient subduction-modified mantle, likely of Caledonian origin, that were tectonically reactivated and exhumed during rifting.

Overlying Unit 2, a thin (~50 cm thick) layer of tectonized gabbro layer separates the serpentinized basement from the overlying volcano-sedimentary units. Downhole, deformation fabrics evolve from brittle overprinting to pervasive ductile mylonitization, consistent with progressive exhumation along a detachment fault zone (Tucholke et al., 2007).

Although syn-rift magmatism was volumetrically minor, late-stage gabbroic intrusions are observed within Unit 2. These crosscutting veins consist of (a) zircon- and Cl-apatite-bearing plagioclase hornblende veins and (b) plagioclase, amphibole, and ilmenite, indicating variable degrees of metasomatic interaction with the host peridotite (Müntener & Manatschal, 2006; Tucholke et al., 2007). Radiometric ages constrain the age of magmatism to ~128–113 Ma (Jagoutz et al., 2007), interpreted as localized melt generation and injection during the late rifting and incipient seafloor spreading phases.

Carbonation is widespread in both Units 1 and 2. Vein networks composed predominantly of calcite often exhibit crack-seal textures, indicative of repeated episodes of fracturing and fluid influx. Stable isotope data and petrographic evidence suggest that these carbonates formed at low temperatures (<50°C, Picazo et al., 2019), during late-stage seawater-related hydrothermal alteration. Carbonation occurs along the fluid pathways and fractures associated with serpentinization reactions and locally overprints earlier hydration features (Kodolányi et al., 2012; Vesin et al., 2023).

3. Analytical Methods

Major element compositions of minerals were obtained using the Electron Probe MicroAnalyzer (EPMA) JEOL JXA8200 Super Probe operating at the University of Milan (Italy). An accelerating voltage of 15 kV was applied for all analyses. All minerals were measured using a beam current of 15 nA and 1 μm beam size. The counting time was 30 s for peak and 10 s for background.

Mineral trace element compositions were determined at Géosciences Montpellier (AETE-ISO facility, Montpellier University) using a Thermo Scientific Element 2XR (eXtended Range) high resolution Inductively Coupled Plasma Mass Spectrometer (ICP-MS) coupled with a laser ablation (LA) system, and a Microlas (Geolas Q +) automated platform with a 193 nm Excimer Compex 102 laser from LambdaPhysik. The laser energy density was set to 2 J/cm^2 and ablation frequency to 10 Hz.

Raw data were reduced with the GLITTER software package (van Achterberg et al., 2001) using the linear fit to ratio method. Concentrations were determined against the NIST 612 rhyolitic glass using the values from Pearce et al. (1997), and internal standardization relative to EPMA data was done using ^{29}Si for orthopyroxene and ^{43}Ca for clinopyroxene.

For data collection, the largest and freshest mineral grains available in each sample were carefully selected under an optical microscope. Laser spot sizes were optimized to maximize signal intensity while ensuring that only preserved serpentine-free mineral domains were analyzed. Spot diameters were set to 110 μm for orthopyroxene and 50 μm for clinopyroxene. Following analysis, each ablation site was systematically re-examined to verify the absence of alteration. During data reduction, signals were further filtered for spikes on an element-by-element basis. These combined procedures ensure that the reported compositions faithfully represent primary mantle mineral chemistry.

Instrument sensitivity related to analytical conditions was determined from the average across all days of repeat measurements of NIST 612. Reference basalt BIR-1G was used to monitor accuracy and reproducibility within a single series and between runs (Table S1 in Supporting Information S1). Accuracy and reproducibility were expressed, respectively, as the relative deviation (%) of the mean measured BIR-1G concentrations from the

15252027, 2026, 10, Downloaded from https://agupubs.onlinelibrary.wiley.com/doi/10.1029/2026GC013203 by CochraneItalia, Wiley Online Library on [07/10/2026]. See the Terms and Conditions (https://onlinelibrary.wiley.com/terms-and-conditions) on Wiley Online Library for rules of use; OA articles are governed by the applicable Creative Commons License

GEOREM preferred values and as the relative standard deviation (RSD, %) of replicate BIR-1G analyses. For the data set, reproducibility was better than 5% for most elements except for Li (~10%) and Sc (~8%) and for the most incompatible elements (<50 ng/g), such as Cs (~30%), Th, and U (~10%). Overall, measured values were comparable within analytical uncertainties to GEOREM accepted values (Jochum et al., 2005).

4. Results

4.1. Sample Description and Petrography

This study focuses on mantle rocks recovered during ODP Leg 210, specifically from Hole 1277A. Out of nine collected samples (Figure S2 in Supporting Information S1), eight were selected for detailed petrographic and mineralogical analysis. The studied lithologies are serpentinized peridotites from the mantle basement (Figure S1 in Supporting Information S1). The downhole location of the samples, along with the primary mineral assemblage and main textural features, is summarized in Table 1 and illustrated in Figure S2 in Supporting Information S1.

All samples exhibit a high degree of serpentinization visually estimated at 85%–90% based on thin-section petrography. Despite this extensive serpentinization, pseudomorphic replacements after olivine and pyroxenes enable the identification of the protoliths as spinel-harzburgites, containing ≤2 vol.% clinopyroxene. Texturally, the spinel harzburgites are mylonitic (Figure 2a), consisting mainly of orthopyroxene + spinel porphyroclasts set in a fine-grained mylonitic matrix, now almost completely serpentinized (Figures 2b and 2c).

Olivine porphyroclasts are entirely replaced by serpentine ± magnetite, forming a well-developed mesh-like texture. Porphyroclastic orthopyroxene, up to 4–5 mm in size, exhibits variable shapes from rounded, folded to strongly elongated (Figures 2a, 2b and 2d). Extremely stretched porphyroclasts with a high aspect ratio up to ~20:1 were also observed (Figure 2a).

Orthopyroxene has been significantly affected by pseudomorphic crystallization of serpentinite, resulting in a bastite texture. Relict fresh, exsolved orthopyroxene is commonly preserved in the cores of large bastite grains. In the most altered samples, carbonate (calcite) locally surrounds (Figure 2e) or completely replaces bastite grains, whereas in the mylonitic matrix, orthopyroxene is entirely replaced by serpentine and/or calcite.

Clinopyroxene is scarce (≤2 vol.%) and shows a primary phase texture only in harzburgite 1277-1. In the other samples, clinopyroxene occurs as small grains (~20–80 μm), typically developing along irregular orthopyroxene boundaries (Figure 2f) or in association with spinel in vermicular intergrowths (Figure 3e). Clinopyroxene estimated modal abundance includes both preserved grains and altered grains that can be confidently identified as pseudomorphs after clinopyroxene based on their smaller grain size and distinct alteration style relative to orthopyroxene. Except for clinopyroxene associated with spinel, the textural setting and grain size make it difficult to unequivocally assess whether these occurrences represent remnants of primary clinopyroxene or secondary clinopyroxene (i.e., precipitated from a melt). Accordingly, no distinction is made between different clinopyroxene types.

Spinel is ubiquitous. It is brown, or dark brown to reddish in color, and displays a wide range of sizes and textures. Spinel porphyroclasts are commonly mm-sized (~0.5–4 mm), showing irregular to holly-leaf shapes (Figures 3a and 3b). In most samples, spinel grains are markedly elongated and arranged in trails parallel to the rock foliation.

Three main textural types are distinguished:

1. Vermicular spinel, occurring either as isolated grains dispersed within the (serpentinized) mylonitic matrix (Figure 3c) or as thin rims outlining the edge of orthopyroxene porphyroclasts (Figure 3d).
2. Clinopyroxene + spinel symplectites, forming intergrowths (Figure 3e) that develop along (serpentinized) olivine porphyroclasts. In this sub-type, clinopyroxene is often replaced by amphibole (see also below).
3. Orthopyroxene + spinel symplectites (Figures 3f–3h), typically composed of orthopyroxene (now altered into calcite), spinel and, locally, minor clinopyroxene. These intergrowths are mostly confined to the outlines of the (serpentinized) olivine porphyroclasts.

These spinel textures display striking similarities to those described in highly depleted peridotites from modern slow-spreading ridge settings (e.g., Suhr et al., 2008). In the investigated samples, symplectitic intergrowths are commonly stretched and aligned parallel to foliation.

15252027, 2026, 10, Downloaded from https://agupubs.onlinelibrary.wiley.com/doi/10.1029/2026GC013203 by CochraneItalia, Wiley Online Library on [07/10/2026]. See the Terms and Conditions (https://onlinelibrary.wiley.com/terms-and-conditions) on Wiley Online Library for rules of use; OA articles are governed by the applicable Creative Commons License

Table 1
Sample Names and Their Positions in ODP Cores

Sample name	Core	Section	Interval (cm)	Depht (mbsf)	Mantle assemblage
1277–1	6	1	98–103	143.08	Opx, Spl, Cpx
1277–2	8	1	91–94	162.41	Serpentinized[a]
1277–3	8	1	118–122.5	162.68	Opx, Spl
1277–4	8	2	18–22	163.13	Opx, Spl, Cpx
1277–5	9	1	117–121	171.87	Opx, Spl
1277–6	9	4	94–97	175.95	Opx, Cpx, Spl
1277–7	9	5	99–103	177.41	Opx, Spl
1277–8	9	6	55–60	178.27	Opx, Spl

Note. All the studied rock-types are spinel harzburgites from ODP Leg 210, Hole 1277A. [a]No primary mantle phases preserved.

Pale brown prismatic amphiboles, cutting or rimming pyroxene relics (Figures S3a and S3b in Supporting Information S1), are commonly found in the studied peridotites. It also occurs as prismatic crystals (Figure S3c in Supporting Information S1), often replacing clinopyroxene on holly leaf-shaped spinels or within symplectitic intergrowths (Figures 3b and 3f). Pale green amphibole with needle-like shapes was also documented in several samples. Although widespread, amphibole occurs at very low modal abundance. Its abundance was not quantitatively determined; however, even if entirely considered as a replacement product after clinopyroxene, it would not significantly affect the estimated clinopyroxene modal abundance.

Multiple vein generations were recognized in the investigated samples: (a) early serpentine veins crosscutting mesh and bastite textures (Figure 2a; Figures S2, S3d, and S3e in Supporting Information S1), and (b) late-stage carbonate veins (Figure S3f in Supporting Information S1). Carbonate veining and replacive calcite within bastite were also described by Kodolányi et al. (2012), who attributed these features to late seafloor weathering.

4.2. Major Element Mineral Chemistry

The major element compositions of the analyzed mineral phases are reported in Table S2.

Orthopyroxene (Figure 4) is characterized by high and variable Mg# values (0.910–0.925, Figure 4a). Al_2O_3 contents are low (2.36–3.19 wt.%) and show a positive correlation with Cr_2O_3 (0.57–1.05 wt.%, Figure 4b). CaO is also low to moderate, ranging from 0.57 to 1.39 wt.% (Table S2).

As shown in Figure 4, the studied samples show major element systematics comparable to abyssal peridotites (Warren, 2016), but tend to plot at the more depleted compositional spectrum. The new data also extend the previously reported compositional field of NFM peridotites (Müntener & Manatschal, 2006) toward more refractory compositions. Overall, the NFM peridotites define a more restricted compositional range than the WIM samples, overlapping with their most refractory compositions but extending to even more depleted values.

Clinopyroxene is characterized by refractory compositions (Table S2), as indicated by low Al_2O_3 (1.48–2.98 wt.%) and Na_2O (0.06–0.37 wt.%) contents, coupled with elevated Mg# values (0.935–0.947). TiO_2 contents are invariably <0.10 wt.% and sometimes below detection limit. These compositions generally fall toward the depleted end of, or extend to lower Al_2O_3 contents than, the compositional range reported for abyssal peridotites (Al_2O_3 = 2.7–8.2 wt.%; Na_2O = 0.05–1.72 wt.%; e.g., Warren, 2016).

Spinel compositions span nearly the full range observed in abyssal peridotites, displaying considerable variation in Cr# (0.317–0.523, Figure 5a). TiO_2 contents are generally <0.10 wt.% (Figure 5b) and fall below detection limits in most samples. Compared to published data for NFM peridotites (Müntener & Manatschal, 2006), the investigated samples largely overlap the previously reported compositional fields, while slightly extending toward lower Cr#. Consistent with orthopyroxene, the overall compositional range of the NFM peridotites remains more restricted than that of WIM peridotites. In addition, WIM samples show more frequent deviation from the mantle array (Figure 5a) and systematically higher TiO_2 contents for a given Cr# (Figure 5b).

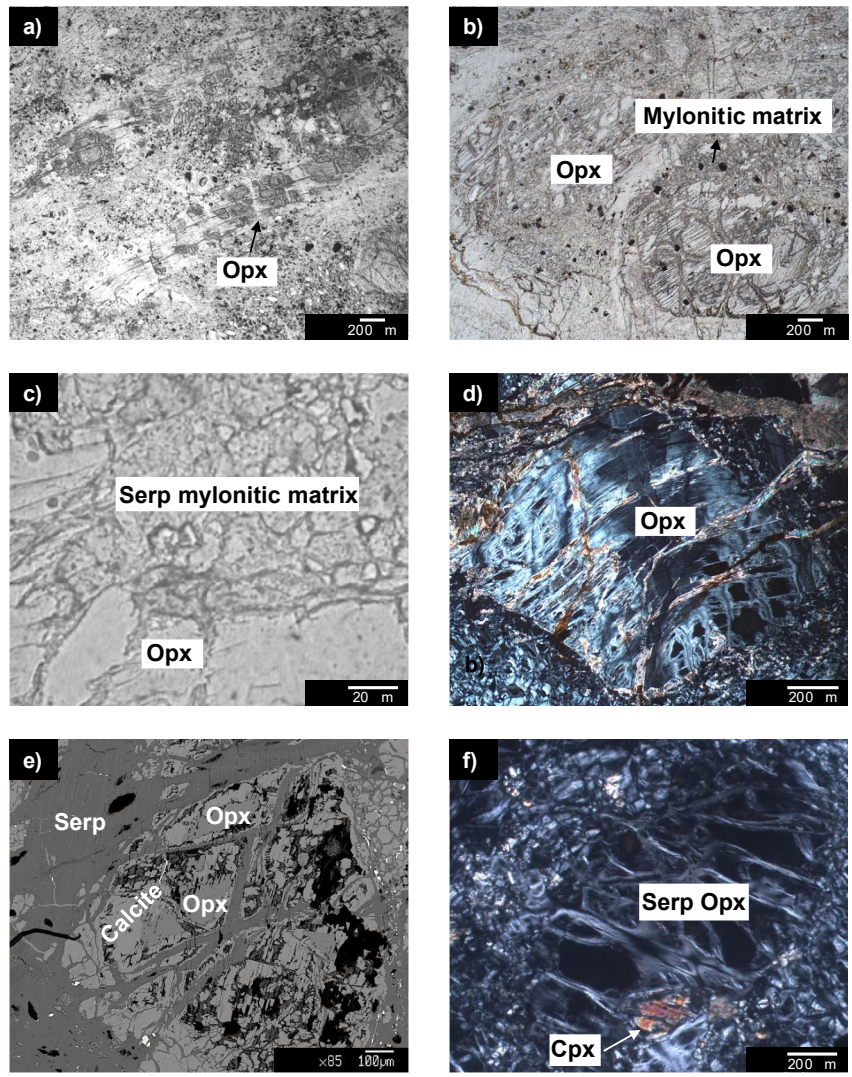


Figure 2. Representative microtextural features of the NFM peridotites. (a) Mylonitic texture with stretched orthopyroxene porphyroclasts in a fine-grained matrix (1277-7); (b) rounded orthopyroxene porphyroclasts in a serpentinized mylonitic matrix (1277-6); (c) serpentinized mylonitic matrix surrounding orthopyroxene porphyroclast (1277-1); (d) folded, serpentinized orthopyroxene porphyroclast (1277-1); (e) BSE image showing fresh orthopyroxene domains preserved within an altered, calcitized porphyroclast (1277-3); (f) clinopyroxene within a serpentinized orthopyroxene embayment (1277-6).

Amphibole has been identified in five harzburgites (1277-1, 1277-3, 1277-5, 1277-6, and 1277-7). According to the classification of Leake et al. (1997), amphibole compositions range from Mg-hornblende (only present in 1277-3 and 1277-7) to tremolite (Figure S4 in Supporting Information S1). Mg-hornblende is characterized by elevated Al_2O_3 (up to 13.31 wt.%) and Na_2O (1.33–1.80 wt.%) contents, associated to low TiO_2 concentrations (up to 0.32 wt.%), sometimes below detection limit. Tremolitic amphibole displays markedly lower Al_2O_3 (1.20–5.73 wt.%) and Na_2O (0.18–0.63 wt.%) contents, with TiO_2 typically below the detection limit.

4.3. In-Situ Trace Element Chemistry

In situ trace element compositions of ortho- and clinopyroxene are listed in Table S3 and illustrated in Figure 6.

Orthopyroxene displays concave downward REE patterns (Figure 6a), characterized by low Yb_N (0.04–0.8) and steeply plunging HREE (Dy_N/Yb_N = 0.05–0.23). Two harzburgites (1277-4 and 1277-7) show selective LREE

15252027, 2026, 10, Downloaded from https://agupubs.onlinelibrary.wiley.com/doi/10.1029/2026GC013203 by CochraneItalia, Wiley Online Library on [07/10/2026]. See the Terms and Conditions (https://onlinelibrary.wiley.com/terms-and-conditions) on Wiley Online Library for rules of use; OA articles are governed by the applicable Creative Commons License

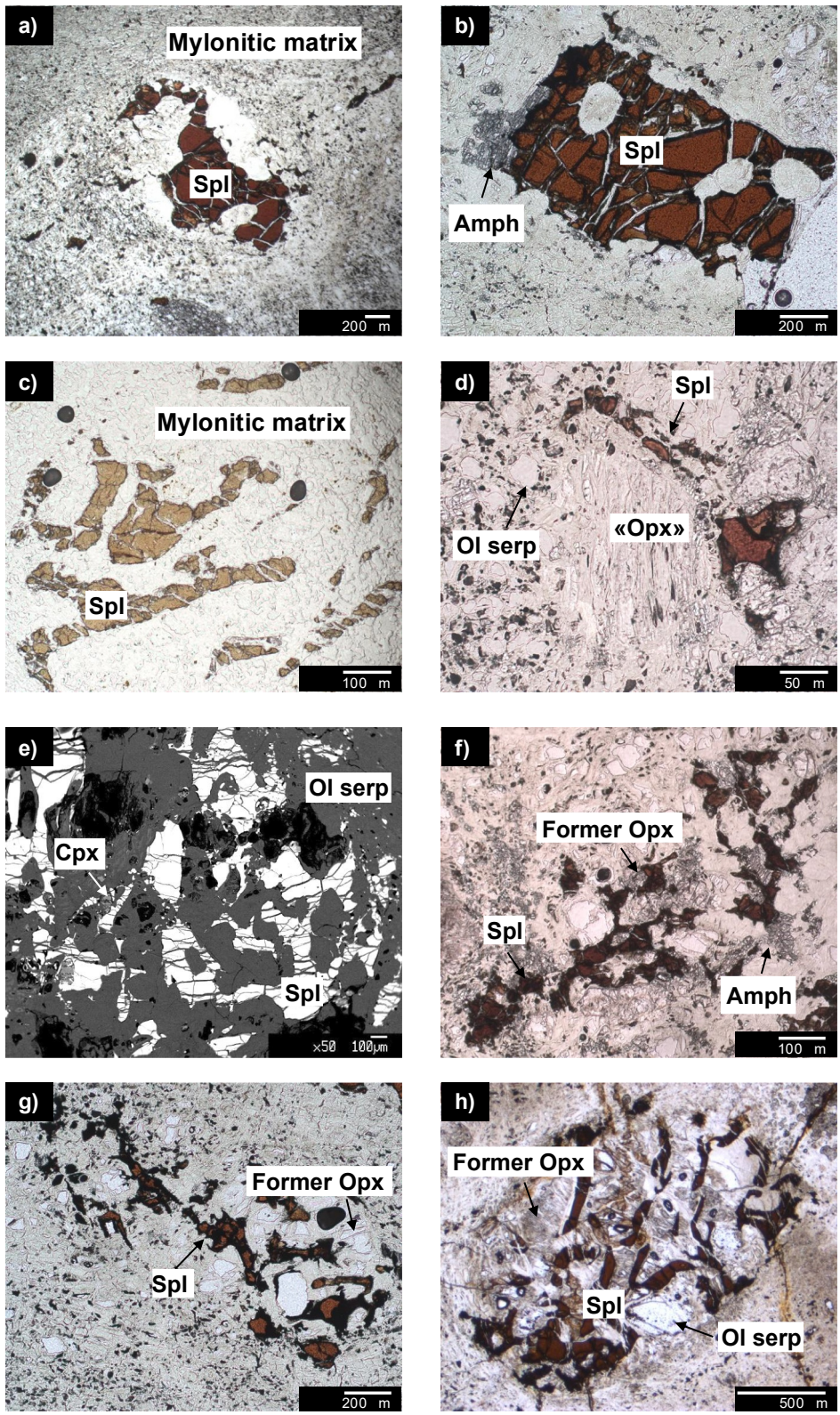


Figure 3.

15252027, 2026, 10, Downloaded from https://agupubs.onlinelibrary.wiley.com/doi/10.1029/2026GC013203 by CochraneItalia, Wiley Online Library on [07/10/2026]. See the Terms and Conditions (https://onlinelibrary.wiley.com/terms-and-conditions) on Wiley Online Library for rules of use; OA articles are governed by the applicable Creative Commons License

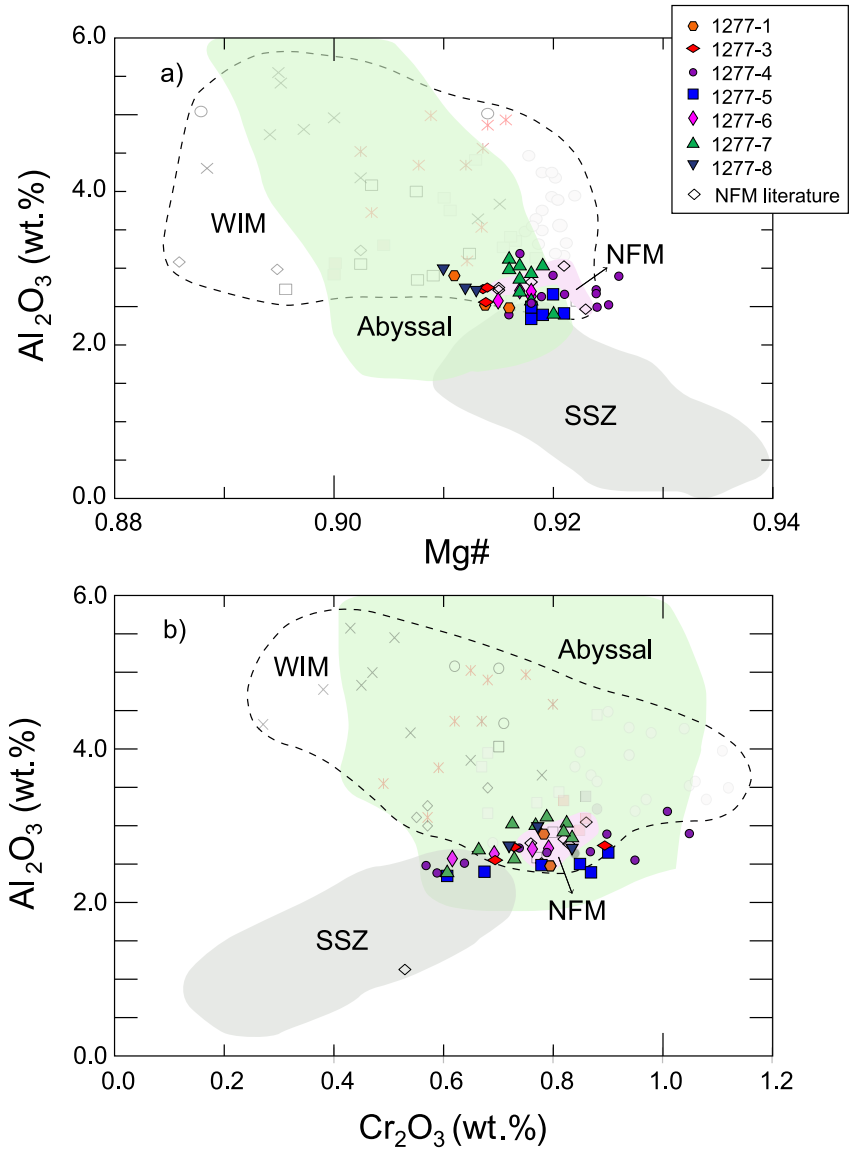


Figure 4. Orthopyroxene major element variations. (a) Mg# versus Al_2O_3 (wt.%); (b) Cr_2O_3 (wt.%) versus Al_2O_3 (wt.%). Reported fields: green = abyssal peridotites (Warren, 2016); gray = supra-subduction zone mantle: Izu-Bonin Mariana (Nishio et al., 2026; Parkinson & Pearce, 1998), New Caldonia (Secchiari et al., 2020), Tonga (Birner et al., 2017), Papua New Guinea (Barrett et al., 2022); pink = NFM peridotites (Müntener & Manatschal, 2006). West Iberian margin (WIM) field (dashed line) = literature data of the WIM peridotites. Spinel peridotites: cross = Galicia Bank dives (Chazot et al., 2005); empty squares = Hole 899B (Chazot et al., 2005); red squares = Hole 899B reactive harzburgites (Secchiari et al., 2025); circles = Hole 1070A (Abe, 2001; Hébert et al., 2001); gray circles = Hole 1070A harzburgites (Secchiari et al., 2025); diamond = Hole 897C and 897D (Cornen et al., 1996). Plagioclase peridotites: red asterisk = Galicia margin (Kornprobst & Tabit, 1988); triangle = Hole 1068A (Abe, 2001).

enrichment (La_N/Nd_N = 1.81–5.53), whereas LREE and MREE are generally below the detection limit in the other samples. Compared to published data for WIM peridotites, the analyzed samples fall within the lower range of HREE concentrations observed in reactive harzburgites (Hole 899B), extending to even lower values. By

Figure 3. Main spinel morphologies in the NFM peridotites. (a) Holly-leaf-shaped porphyroclast (1277-5); (b) spinel porphyroclast rimmed by tremolite (1277-6); (c) vermicular spinel (1277-1); (d) vermicular spinel overgrowing a strongly serpentinized orthopyroxene porphyroclast (1277-7); (e) BSE image showing intricate spinel + clinopyroxene intergrowths along serpentinized olivine porphyroclasts (1277-3); (f) symplectitic intergrowths of orthopyroxene (completely replaced by calcite), spinel and clinopyroxene (altered to tremolite, 1277-7); (g, h) spinel- altered orthopyroxene symplectites (1277-6 and 1277-1).

15252027, 2026, 10, Downloaded from https://agupubs.onlinelibrary.wiley.com/doi/10.1029/2026GC013203 by CochraneItalia, Wiley Online Library on [07/10/2026]. See the Terms and Conditions (https://onlinelibrary.wiley.com/terms-and-conditions) on Wiley Online Library for rules of use; OA articles are governed by the applicable Creative Commons License

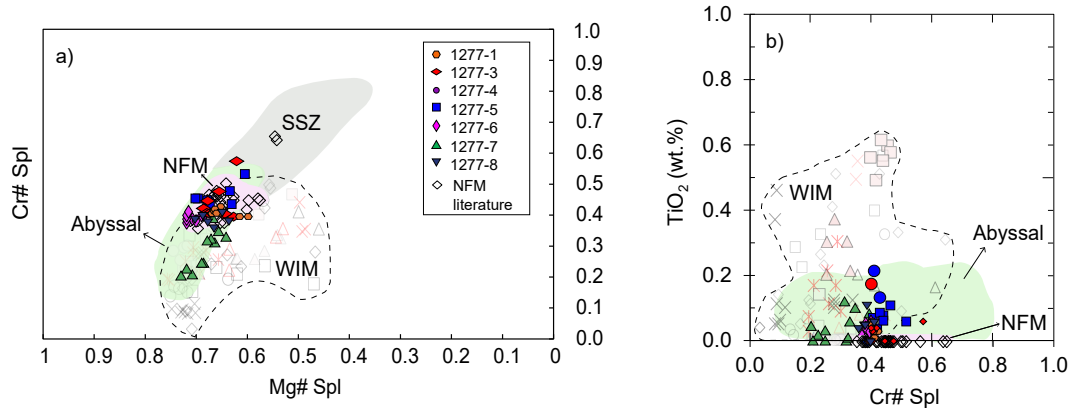


Figure 5. Compositional variations of spinel. (a) Cr# versus Mg#. Field for abyssal and forearc peridotites are from Dick and Bullen (1984) and Ishii et al. (1992); (b) spinel Cr# versus TiO_2 (wt.%). Reported for comparison: pink = NFM peridotites (Müntener & Manatschal, 2006); dashed line = West Iberian margin peridotites as in Figure 4.

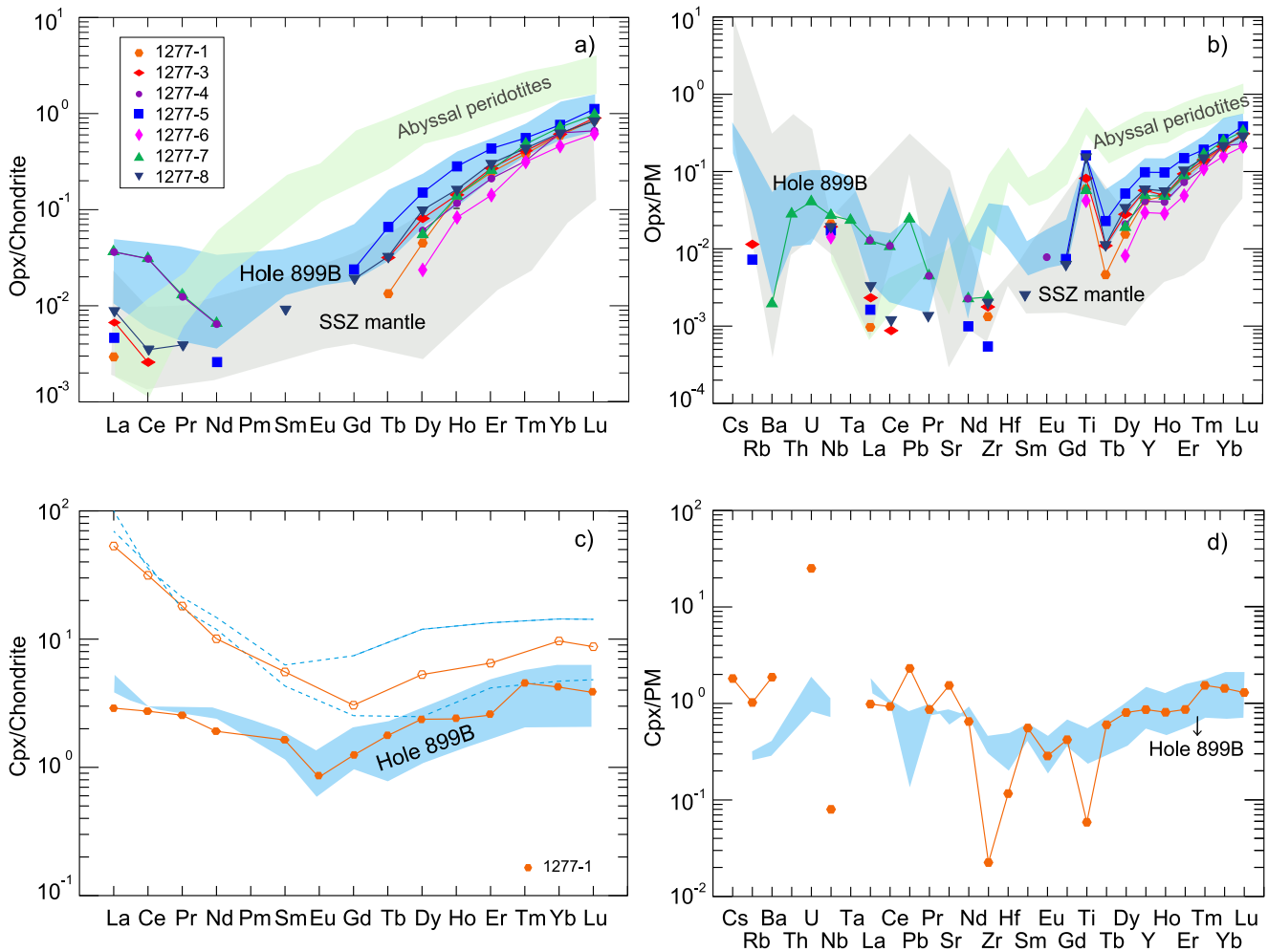


Figure 6. Average orthopyroxene and clinopyroxene trace element patterns. (a and c) Chondrite-normalized REE patterns; (b and d) PM-normalized extended trace element patterns. Normalizing values after Sun and McDonough (1989). Fields reported for comparison: blue = Hole 899B reactive harzburgites (West Iberian margin, Secchiari et al., 2025); gray = supra-subduction zone peridotites (Barrett et al., 2022; Birner et al., 2017; Nishio et al., 2026; Secchiari et al., 2020); green = abyssal peridotites (D'Errico et al., 2016; Harigane et al., 2022). Empty symbols in panel (c) are melt in equilibrium with 1277-1 clinopyroxene calculated using partition coefficients of Hart and Dunn (1993). Melts in equilibrium with clinopyroxene of Hole 899B harzburgites (blue dashed lines) are reported for comparison.

15252027, 2026, 10, Downloaded from https://agupubs.onlinelibrary.wiley.com/doi/10.1029/2026GC013203 by CochraneItalia, Wiley Online Library on [07/10/2026]. See the Terms and Conditions (https://onlinelibrary.wiley.com/terms-and-conditions) on Wiley Online Library for rules of use; OA articles are governed by the applicable Creative Commons License

15252027, 2026, 10, Downloaded from https://agupubs.onlinelibrary.wiley.com/doi/10.1029/2026GC013203 by CochraneItalia, Wiley Online Library on [07/10/2026]. See the Terms and Conditions (https://onlinelibrary.wiley.com/terms-and-conditions) on Wiley Online Library for rules of use; OA articles are governed by the applicable Creative Commons License

contrast, the investigated samples appear notably more depleted than abyssal peridotites (e.g., D'Errico et al., 2016; Harigane et al., 2022).

Primitive mantle (PM)-normalized extended trace element patterns (Figure 6b) reveal extremely low concentrations in orthopyroxene (0.0005–0.3 PM-values), with most incompatible elements below detection limits. HFSE (i.e., high field strength elements) are strongly depleted, showing extremely low Zr abundances ($\sim 10^{-4}$–10^{-3} PM-values), whereas Hf is invariably below detection limit.

Primary clinopyroxene was only found and analyzed in one sample (1277-1, Figures 6c and 6d). It displays a V-shaped (La/Sm_N = 4.3; La_N = 2.9) chondrite-normalized REE pattern, characterized by low HREE (Yb_N = 4.2) and a weak negative Eu anomaly (Figure 6c). This pattern closely resembles those of reactive spinel harzburgites from the WIM (Hole 899B; Secchiari et al., 2025) and mantle xenoliths from central and eastern Europe (Downes, 2001; Downes et al., 2003). PM-normalized extended trace element diagram (Figure 6d) shows concentrations ranging between 0.02 and 2 PM-values. The most incompatible elements (LILE and HFSE) exhibit the lowest absolute abundances and are in some cases below detection limits. Zr and Ti are strikingly depleted relative to the neighboring elements.

4.4. Geothermometry

Notwithstanding the strongly serpentinized nature of the investigated samples, equilibrium temperatures could be obtained for relict mineral domains. The equilibrium temperatures calculated for the studied peridotites are reported in Table S4 in Supporting Information S1.

Specifically, we employed: (a) a REE-in-two-pyroxene thermometer ($T_{REE\text{-}Y}$, Liang et al., 2013), (b) two-pyroxene solvus thermometer (T_{BKN}, Brey & Köhler, 1990), and (c) a cation exchange thermometer Ca-in-orthopyroxene ($T_{Ca\text{-}in\text{-}Opx}$, Brey & Köhler, 1990). Calculations were restricted to fresh, well-preserved mineral analyses, and pressure was fixed at 10 kbar.

Application of the REE-in-two-pyroxene thermometer to harzburgite 1277-1, the only sample preserving primary clinopyroxene in equilibrium with orthopyroxene (Figure S5 in Supporting Information S1), yielded a temperature of 940 ± 20°C. Slightly lower values were obtained for the same harzburgite using the two-pyroxene solvus thermometer T_{BKN} = 833°C.

Calculation of $T_{Ca\text{-}in\text{-}Opx}$ (Brey & Köhler, 1990) was possible for all the samples in our data set, yielding a relatively narrow range of temperatures between 912°C and 983°C. These values represent minimum equilibrium temperatures, assuming that orthopyroxene compositions reflect equilibrium with clinopyroxene. This assumption is reasonable, as cooling of an initially clinopyroxene-undersaturated assemblage and subsolidus Ca exchange with olivine would promote clinopyroxene saturation (Lindsley, 1983). Consistently, clinopyroxene exsolution lamellae are widely observed in preserved orthopyroxene cores from the analyzed harzburgites.

5. Discussion

5.1. Pre-Serpentinization Depletion History

The petrological and geochemical characters of the NFM peridotites indicate a history of melt depletion prior to serpentinization, resulting in refractory compositions.

Petrographic observations show mineral modes dominated by olivine and orthopyroxene, with only minor amounts of clinopyroxene preserved in the investigated harzburgites. However, pervasive serpentinization hampers a robust assessment of primary modal abundance. The limited occurrence of clinopyroxene is consistent with high degrees of melt extraction approaching clinopyroxene exhaustion, in agreement with constraints from mineral chemistry.

The major element composition of orthopyroxene is characterized by high Mg# coupled to low Al_2O_3 contents, typical of melt residues, while spinel systematically shows high Cr#. Using the calibration of Hellebrand et al. (2001), we derived degrees of partial melting (F) from spinel Cr#, obtaining F ranging between 13% and 18%. However, spinel Cr# can be easily modified by later melt–rock interactions and may not fully capture the depletion history of the investigated samples.

15252027, 2026, 10, Downloaded from https://agupubs.onlinelibrary.wiley.com/doi/10.1029/2026GC013203 by CochraneItalia, Wiley Online Library on [07/10/2026]. See the Terms and Conditions (https://onlinelibrary.wiley.com/terms-and-conditions) on Wiley Online Library for rules of use; OA articles are governed by the applicable Creative Commons License

Previous studies have shown that in highly refractory, cpx-poor to cpx-free harzburgites, orthopyroxene provides a robust proxy for constraining the degree of partial melting and identifying subsequent melt-rock interaction processes (D'Errico et al., 2016; Scott et al., 2016). We therefore performed geochemical modeling based on orthopyroxene REE compositions, to obtain more robust estimates of the extent of partial melting. Details of the modeling, including partition coefficients and the starting mantle source compositions are reported in Table S5 in Supporting Information S1. Fractional melting of a depleted mantle source under spinel-facies conditions fails to reproduce the steep REE patterns and the inter-element fractionation (Figure 7a) observed in the analyzed samples, particularly their relatively low MREE/HREE ratios. Such fractionation is characteristic of peridotites that experienced an initial stage of melting in the presence of residual garnet (Hellebrand et al., 2002). We thus simulate polybaric fractional melting of a depleted mantle source beginning in the garnet stability field and continuing in the spinel peridotite field (Figure 7b).

Orthopyroxene chondrite-normalized REE patterns in the studied harzburgites are broadly sub-parallel, with sample 1277-6 showing the lowest absolute REE concentrations. For this harzburgite, the melting curves reproduce the HREE concentrations with ∼5% melting in the garnet stability field followed by ∼ 9% additional melting in the spinel field. By contrast, the higher HREE concentrations observed in other samples would imply lower apparent degrees of partial melting, differing by up to ∼3% within the spinel field (Figure 7b). These variations occur over meter-scale distances (see sample location in Figure S1 in Supporting Information S1) and would imply significant temperature gradients on an unrealistically short spatial scale. As emphasized in previous studies, this type of small-scale heterogeneity is unlikely to reflect real differences in the degree of melt extraction in the mantle column but rather record local melt infiltration and reactive exchanges with the host peridotite (e.g., D'Errico et al., 2016).

We thus assume the melting degree recorded by sample 1277-6 as a minimum estimate of the overall melt depletion experienced by the NFM peridotites, while inter-sample variability is best explained by secondary enrichment, likely linked to melt-rock interaction (see following section).

The onset of melting in the garnet stability field at ∼80–90 km depth implies either elevated mantle potential temperatures or local compositional heterogeneities in the pre-rift mantle source (Brunelli et al., 2006). Such conditions are inconsistent with simple lithospheric thinning during Jurassic rifting and instead point to a previous melting episode predating the recent rifting evolution. This interpretation aligns with previous studies on peridotites from magma-poor passive margins and slow- to ultraslow spreading ridges, where evidence for inherited pre-rift melt depletion is also recorded (Hellebrand et al., 2002; Seyler et al., 2011). Comparable signatures have also been reported in the conjugate WIM, where possibly ancient high-degree melting was subsequently overprinted by rift-related melt-rock interactions (Chazot et al., 2005; Secchiari et al., 2025). Taken together, these findings reconcile the highly refractory nature of the NFM peridotites with their limited melt productivity and provide a coherent explanation for the scarcity of magmatic products in the lithological record of the Iberia-Newfoundland conjugate margin (e.g., Jagoutz et al., 2007 and references therein).

5.2. Post Melting Evolution of the NFM Peridotites

5.2.1. Metasomatism Operated by Enriched Melts

Although the NFM peridotites preserve clear evidence of high-degree melt depletion, several petrographic, mineralogical, and geochemical features indicate subsequent modification by melt-rock interaction.

The first indication comes from the modal composition of the investigated lithologies. Despite pervasive serpentinization, clinopyroxene is systematically less abundant than expected for the estimated melting degrees. This discrepancy suggests that the calculated melt extraction rates are underestimated and that mineral compositions record not only melting but also later re-enrichment associated with melt infiltration.

Additional evidence for post-melting processes is provided by trace element systematics in coexisting pyroxenes. Orthopyroxene and clinopyroxene display clear disequilibrium for LREE, and to some extent, for MREE, as indicated by their contrasting chondrite-normalized REE patterns (Figures 6a and 6c) and calculated orthopyroxene/clinopyroxene partition coefficients (Figure S5 in Supporting Information S1).

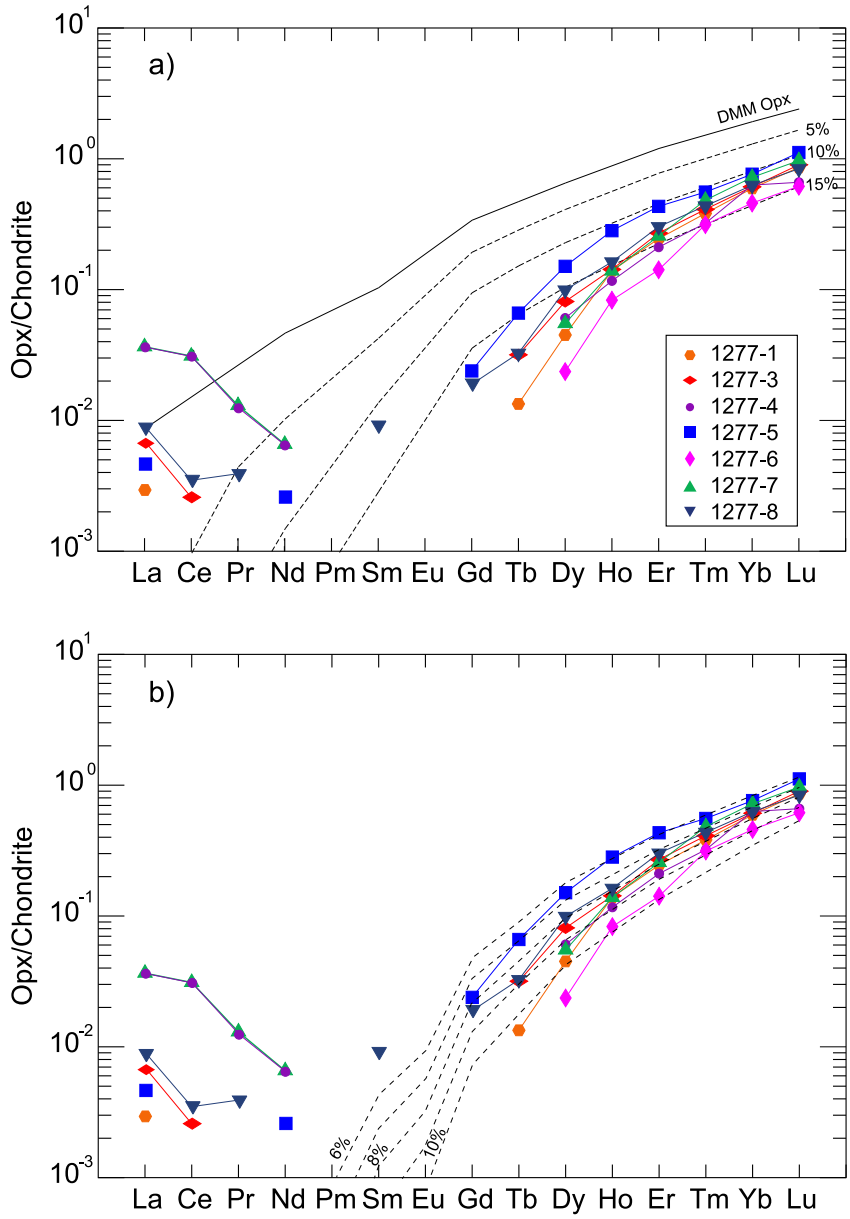


Figure 7. Results of fractional melting modeling for orthopyroxene. Chondrite-normalized REE patterns of residual orthopyroxene produced by non-modal fractional melting: (a) in the spinel stability field, starting from a DMM source (Salters & Stracke, 2004); (b) following 5% melting in the garnet stability field and subsequent melting in the spinel stability field. Numbers next to dashed curves indicate the degree of spinel-facies melting in (a), and the degree of spinel-facies melting following 5% garnet-facies melting in panel (b).

This disequilibrium may reflect either (a) diffusion-controlled re-equilibration during melt percolation, whereby differential diffusivities of REEs lead to incomplete equilibration between coexisting phases, or (b) incomplete melt extraction and retention of low-volume melt fractions, resulting in limited melt–mineral re-equilibration.

Reactive melt percolation is expected to produce chromatographic fractionation of trace elements, whereby the most incompatible elements are controlled by the percolating melt, whereas less incompatible elements remain buffered by the residual peridotite (Godard et al., 1995; Vernières et al., 1997). In contrast, melt retention promotes crystallization of interstitial phases such as clinopyroxene (Hellebrand et al., 2002; Seyler et al., 2001), leading to overall enrichment in incompatible elements.

15252027, 2026, 10, Downloaded from https://agupubs.onlinelibrary.wiley.com/doi/10.1029/2026GC013203 by CochraneItalia, Wiley Online Library on [07/10/2026]. See the Terms and Conditions (https://onlinelibrary.wiley.com/terms-and-conditions) on Wiley Online Library for rules of use; OA articles are governed by the applicable Creative Commons License

15252027, 2026, 10, Downloaded from https://agupubs.onlinelibrary.wiley.com/doi/10.1029/2026GC013203 by CochraneItalia, Wiley Online Library on [07/10/2026]. See the Terms and Conditions (https://onlinelibrary.wiley.com/terms-and-conditions) on Wiley Online Library for rules of use; OA articles are governed by the applicable Creative Commons License

Although incomplete melt extraction cannot be ruled out, the observed trace variations are more consistent with the first scenario. In particular, the decoupling between LREE-MREE and HREE in clinopyroxene, the sub-parallel HREE patterns in orthopyroxene and the lack of equilibrium partitioning between pyroxenes are difficult to reconcile with simple melt retention and instead indicate selective redistribution of trace element during melt transport.

HFSE systematics provide further support for this interpretation. Negative anomalies in Ti and Zr are commonly observed in mantle clinopyroxene and have long been debated. Rampone et al. (1991) proposed that positive anomalies in orthopyroxene may compensate for those in clinopyroxene, yielding whole-rock patterns without significant anomalies. However, this model is not consistent with the studied samples, which display pronounced negative Zr anomalies in both clinopyroxene and orthopyroxene, together with strongly depleted Ti. Alternatively, Zr-Hf fractionation has been linked to chromatographic effects during melt percolation at low melt/rock ratios (Niu, 2004). In this framework, strong depletion in Zr and Ti, Zr/Hf fractionation, and LREE enrichment are widely reported in metasomatized mantle xenoliths (Downes et al., 2003; Witt-Eickschen & Kramm, 1997; Xu et al., 2000).These features were interpreted to reflect selective trace element redistribution during reactive melt transport, following high degrees of melt extraction (Downes et al., 2015).

To test this hypothesis, we modeled trace elements characterized with progressively increasing incompatibility (Yb, Er, Ti, Zr), comparing their concentrations in orthopyroxene with partial melting trends (Figure 8). The more compatible elements (Yb, Er) are well reproduced by melting curves involving 5% melting in the garnet stability field followed by melting in the spinel field (Figure 8a), indicating that their abundances largely reflect melt extraction. In contrast, increasingly incompatible elements deviate from melting model predictions: Ti plots at lower concentrations than expected (Figure 8b), whereas Zr shows the strongest mismatch, with several samples plotting at higher concentrations than predicted (Figure 8c). The mismatch between observed and modeled concentrations increases with incompatibility (Yb-Er → Ti → Zr) and culminates in Zr relative enrichment, reflecting selective redistribution of the most incompatible elements during melt percolation. This behavior is consistent with chromatographic fractionation at low melt/rock ratios, whereby highly incompatible elements are transported with the migrating melt, whereas less incompatible elements remain buffered by the residual peridotite (Godard et al., 1995; Vernières et al., 1997).

Additional constraints on the nature of the infiltrating melts are provided by clinopyroxene trace element compositions. Moderate LREE enrichment, combined with low Sr-Ba contents, Th-U-Ta below detection limits, and high Ti/Eu ratios rules out a carbonatitic source for these melts (e.g., Norman, 1998; Scott et al., 2014). Instead, the overall low abundances of incompatible elements, together with LREE-enriched patterns, point to interaction with small volumes of enriched alkaline-like melts.

Modeling melt in equilibrium with the analyzed clinopyroxene, assuming near-equilibrium for the most incompatible elements, yields a moderately LREE-enriched composition (La_N = 53; Figure 7), consistent with infiltration of an enriched melt during the final evolution of the NFM spinel harzburgites. Despite their overall refractory character, the NFM peridotites share with their WIM counterpart a distinctive metasomatic fingerprint, expressed by the uncommon V-shaped REE patterns in clinopyroxene. The occurrence of this rare signature across the conjugate Newfoundland–Iberia margin, as well as in European mantle xenoliths (Downes, 2001; Downes et al., 2003; Ionov et al., 2002), suggests a widespread enrichment event affecting a heterogeneous and variably depleted Variscan SCLM.

Overall, the NFM peridotites record high-degree melt depletion followed by refertilization through low-volume, alkaline-like melts, which imparted this distinctive metasomatic signature prior to Mesozoic rifting and continental breakup.

5.2.2. Origin of the Symplectites: Late Stage-Melt Percolation and Freezing in the Lithospheric Mantle

In addition to the geochemical imprint recorded by ortho- and clinopyroxene, the development of spinel ± pyroxene symplectites provide further evidence for late-stage reactive melt percolation. These symplectitic intergrowths occur along the outlines of serpentinized olivine/orthopyroxene porphyroclasts and within the serpentinized mylonitic matrix (Figure 3), commonly showing elongation and deformation broadly consistent with the rock foliation.

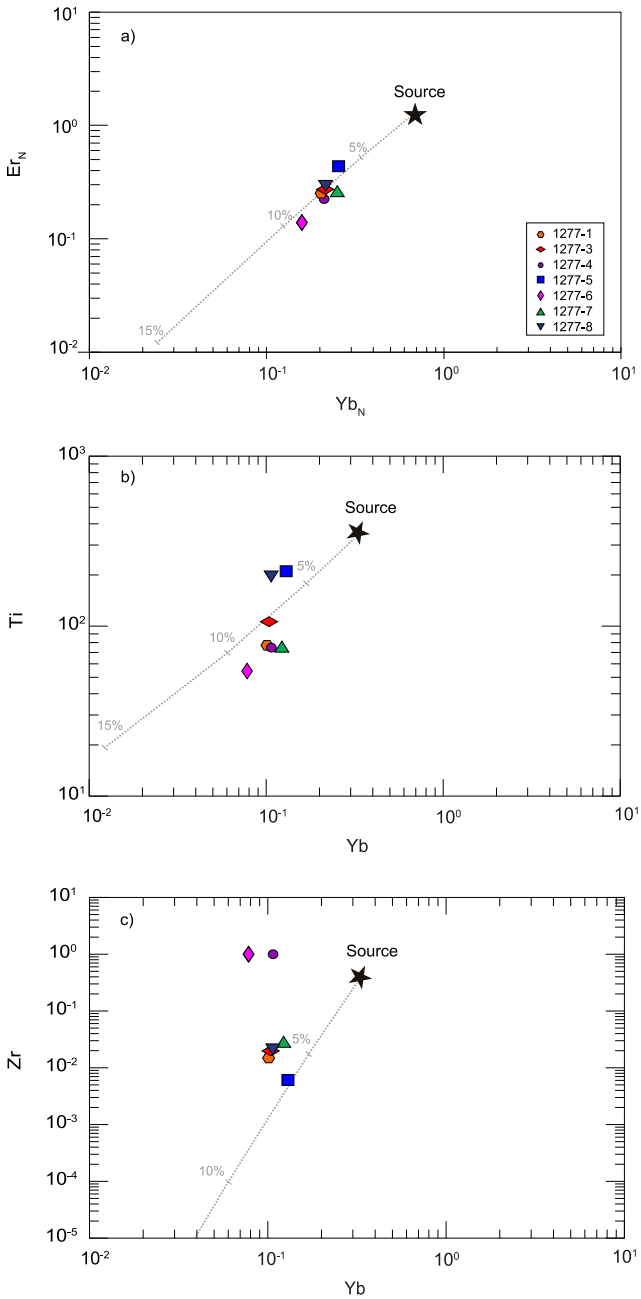


Figure 8. Fractional melting model based upon (a) Er_N–Yb_N, (modified after Norman (1998)), (b) Ti-Yb and (c) Zr-Yb systematics in orthopyroxene. The model calculates non-modal fractional melting in the garnet stability field (5%), followed by 5%, 10%, 15% of melting in the spinel field starting from a DMM mantle source (Salters & Stracke, 2004). Partition coefficients after Ionov et al. (2002).

Similar microtextural features have been described for mantle rocks from both modern and fossil slow-spreading ridges (Dijkstra et al., 2010; Seyler et al., 2007; Suhr et al., 2008). In these peridotites, the development of spinel-clinopyroxene symplectites postdates orthopyroxene-consuming and olivine-precipitating reactions. These microstructures have been interpreted as the result of late stage melt percolation and progressive freezing within a highly depleted harzburgitic matrix. According to Suhr et al. (2008), symplectitic textures in MAR harzburgites record a multistage evolution involving: (a) orthopyroxene resorption coupled with olivine precipitation driven by infiltration of a silica-undersaturated melt, (b) replacement of orthopyroxene by clinopyroxene, and (c) subsequent co-precipitation of spinel and pyroxene from a Cr-saturated, Si-enriched interstitial melt. The symplectitic intergrowths observed in the NFM peridotites show striking similarities to those described in the MAR samples in terms of morphology, mineral assemblages, and microtextural location. Although pervasive serpentinization hampers detailed characterization and limits direct comparison with well-preserved MAR symplectites, the available petrographic evidence supports formation through comparable processes. Similarly, we interpret the NFM symplectites as products of deep and localized melt percolation within a highly depleted mantle matrix. Subsequent melt freezing led to the precipitation of spinel ± pyroxene intergrowths, reflecting diffusion-limited growth under near-solidus conditions during melt consumption and cooling.

An origin from the breakdown of a precursor garnet phase has also been proposed for symplectites (Morishita & Arai, 2003), but appears unlikely for the NFM peridotites. In contrast to those described in Horoman or Tallante peridotites (Morishita & Arai, 2003; Rampone et al., 2009), the symplectites observed in the NFM samples differ markedly in both morphology and textural position. In Horoman or Tallante, symplectites are interpreted as relics of pre-existing garnet and typically occur as rounded fine-grained aggregates enclosed within large orthopyroxene porphyroclasts, with spinel distributed as small, dispersed grains (Morishita & Arai, 2003; Shimizu et al., 2008; Takahashi, 2001).

Moreover, preservation of garnet-bearing domains is unlikely due to the extensive melt extraction experienced by the NFM peridotites, as incongruent melting reactions would have led to early and complete garnet consumption (Walter, 1998).

Taken together, these observations indicate that the NFM symplectites formation reveals a late localized melt–rock reaction event. Their textural features suggest that symplectite formation predated peridotite mylonitization and the onset of strain localization in the lithospheric mantle (see also Section 5.4).

5.3. Origin of the NFM Peridotites: Subduction-Related Mantle or SCLM?

Based on their refractory character and mineral major-element compositions, the NFM peridotites have previously been interpreted as fragments of lithospheric mantle preserving a pre-rift, subduction-related history, possibly inherited from Caledonian or even older orogenic events (e.g., Müntener & Manatschal, 2006). Within this framework, these peridotites were proposed to have been exhumed during rifting of the Iberia-Newfoundland conjugate margin along large-scale shear zones, forming a highly depleted and compositionally buoyant craton-like mantle lithosphere.

The new data presented here allow this interpretation to be reassessed and provide further constraints on the mantle affinity and pre-rift evolution of the NFM peridotites. To this end, we compared their compositions with

15252027, 2026, 10, Downloaded from https://agupubs.onlinelibrary.wiley.com/doi/10.1029/2026GC013203 by CochraneItalia, Wiley Online Library on [07/10/2026]. See the Terms and Conditions (https://onlinelibrary.wiley.com/terms-and-conditions) on Wiley Online Library for rules of use; OA articles are governed by the applicable Creative Commons License

15252027, 2026, 10, Downloaded from https://agupubs.onlinelibrary.wiley.com/doi/10.1029/2026GC013203 by CochraneItalia, Wiley Online Library on [07/10/2026]. See the Terms and Conditions (https://onlinelibrary.wiley.com/terms-and-conditions) on Wiley Online Library for rules of use; OA articles are governed by the applicable Creative Commons License

those of mantle peridotites showing clear evidence of formation in SSZ settings. Given the limited availability of orthopyroxene trace-element data from subduction-related mantle peridotites, the comparison was restricted to peridotite suites for which a SSZ origin is well constrained. These include peridotites from modern forearc settings (Birner et al., 2017; Nishio et al., 2026) and ophiolitic peridotites showing a clear SSZ affinity (Barrett et al., 2022; Secchiari et al., 2020). For the latter, a SSZ origin is further supported by their association with boninitic magmatism (e.g., Cluzel et al., 2016).

Mantle peridotites formed or evolved in subduction related settings typically record high degrees of melt extraction under hydrous conditions, commonly followed by interactions with slab-derived fluids- or hydrous melts (e.g., Parkinson & Pearce, 1998). These processes impart distinctive geochemical signatures, including strong depletion in incompatible elements combined with selective enrichment in fluid mobile elements (e.g., Cs, Rb, Ba, Sr, Pb), and in some cases, slight enrichment in high field strength elements (HFSE), if interaction with melts occurs (Secchiari et al., 2020; Shervais & Jean, 2012).

In contrast, the peridotites drilled in the NFM display geochemical and mineralogical features that differ markedly from those of modern and ophiolitic SSZ peridotites (Figures 4–6). Their slightly higher HREE contents, which only partially overlap with the most enriched SSZ peridotites, together with very low concentrations of Cs, Rb, and Pb, commonly at or below detection limits, are inconsistent with the geochemical signatures expected for subduction-related mantle.

Additional constraints are provided by major element compositions of orthopyroxene and spinel. Both phases in the NFM peridotites are systematically more enriched than their counterparts in SSZ peridotites (Figures 4 and 5), and do not display the extreme depletion typically associated with SSZ environments. This further argues against extensive melting and metasomatism under hydrous subduction-related conditions.

Moreover, geochemical modelling indicates that partial melting of the NFM rocks initiated within the garnet stability field, corresponding to depths of approximately 80–90 km. This contrasts with the typical melting regime in SSZ settings, where hydrous melting predominantly occurs at shallower depths within the spinel stability field (e.g., Shervais et al., 2021). Instead, the NFM peridotites record an earlier episode of dry melting at high pressure, consistent with elevated mantle potential temperatures or upwelling of asthenospheric domains (Brunelli et al., 2006).

This melting event likely predated Jurassic rifting and produced a highly depleted mantle residue. Such inherited depletion would have significantly reduced the melt productivity of the mantle source, thereby limiting melt production during subsequent extension.

Finally, clinopyroxene trace-element systematics indicate interaction with enriched, alkaline-like melts, similar to those documented in the WIM and in mantle xenoliths from central and eastern Europe (Downes, 2001; Secchiari et al., 2025). Alkaline melts are uncommon in SSZ environments but are instead widely associated with metasomatism in SCLM domains (Beard et al., 2002; Cornen et al., 1996; Downes et al., 2003; Ionov et al., 2002; Seifert et al., 1997). The pre-rift timing of these interactions suggests the presence of an enriched mantle source that was later sampled during rifting-related magmatism, including the enriched gabbroic veins cross-cutting the peridotite basement in the NFM (Müntener & Manatschal, 2006; Tucholke & Sibuet, 2007), as well as similarly enriched magmatic products documented in the WIM (Beard et al., 2002; Cornen et al., 1996; Seifert et al., 1997).

5.4. Evolution of the NFM Peridotites: From High Temperature Mantle Processes to Exhumation and Low-Temperature Alteration

The NFM peridotites represent a fragment of SCLM recording a long-lived multistage evolution, from high-temperature mantle processes to subsolidus re-equilibration and retrograde metamorphism during Triassic rifting and exhumation.

The earliest stage of this evolution corresponds to melt extraction under dry conditions, as indicated by the depleted trace element compositions of pyroxene (Figure 6). Partial melting initiated in the garnet stability field and continued at shallower pressures within the spinel peridotite field (Figure 7). This melting episode likely predates Jurassic rifting, as proposed for the WIM peridotites (Chazot et al., 2005; Secchiari et al., 2025), and could account for the strongly refractory character of the NFM mantle section, leaving behind a highly depleted residue with only a minor amount of primary clinopyroxene.

15252027, 2026, 10, Downloaded from https://agupubs.onlinelibrary.wiley.com/doi/10.1029/2026GC013203 by CochraneItalia, Wiley Online Library on [07/10/2026]. See the Terms and Conditions (https://onlinelibrary.wiley.com/terms-and-conditions) on Wiley Online Library for rules of use; OA articles are governed by the applicable Creative Commons License

The presence of refractory mantle domains prior to rifting is consistent with recent geodynamic models emphasizing the role of long-lived lithospheric features in controlling the evolution of the Newfoundland–Iberia system, where mantle inheritance exerts a first-order influence on the geometry and localization of rifting itself (Welford, 2025).

Following melt extraction, geochemical evidence indicates that the NFM peridotites experienced percolation of enriched melts that locally interacted with the host peridotite. We speculate that this metasomatic overprint, highlighted by pyroxene trace element systematics, reflects a post-Variscan or potentially older enrichment event, although its timing cannot be directly constrained from the available data. The occurrence of the atypical, chondrite-normalized clinopyroxene REE-patterns with V-shaped profiles on both sides of the margin, as well as in the European mantle xenoliths, could be tentatively ascribed to a broad re-enrichment event, possibly affecting the SCLM at a regional scale.

The NFM mantle section was subsequently reactivated during Jurassic rifting within large-scale lithospheric shear zones. Progressive extension and exhumation likely promoted limited melt production, with small melt fractions locally stagnating and crystallizing in situ, now preserved as symplectitic intergrowths.

Small melt fractions percolating within the NFM peridotite during rifting may have contributed to the mechanical behavior of the deforming mantle. Experimental and theoretical studies show that even limited volumes of interstitial melt can significantly reduce the effective viscosity of peridotite by enhancing grain-boundary sliding, promoting diffusion creep, and facilitating dynamic recrystallization (Holtzman et al., 2003; Katz et al., 2006). In addition, melt distributed along grain boundaries leads to rock weakening, promoting strain localization and the formation of high-temperature shear zones (Kaczmarek & Müntener, 2008).

In the NFM peridotites, the symplectites are broadly aligned parallel to the main foliation, rather than randomly distributed, suggesting that they did not behave as rigid bodies during ductile deformation. Their occurrence within the mylonitic matrix further indicates that symplectite formation was nearly coeval with grain-size reduction and strain localization.

Thermometric estimates provide constraints on the thermal evolution recorded by the NFM peridotites. Temperatures derived from $T_{Ca\text{-}in\text{-}Opx}$ (910–985°C) are comparable to those obtained by REE-Y thermometry on coexisting pyroxenes ($T_{REE–Y} = 940 \pm 20$°C). The consistency between thermometers calibrated over components with different diffusivity is consistent with relatively slow cooling and prolonged thermal equilibration, in agreement with a long-lived evolution for the NFM mantle section. Such prolonged subsolidus re-equilibration may also have affected the REE compositions of orthopyroxene through trace element redistribution between coexisting pyroxenes. However, the extent of this process is expected to have been limited in the NFM peridotites, given the very low modal abundance of clinopyroxene (≤2 vol.%). Therefore, although some subsolidus modification of orthopyroxene REE compositions cannot be excluded, the overall REE systematics are likely to largely preserve their pre-cooling signature.

As deformation progressed and temperatures decreased, melt mobility was likely progressively reduced. Under such conditions, any transient melt fractions may not have been efficiently extracted toward shallower crustal levels but instead crystallized locally within the peridotite matrix. The resulting spinel-pyroxene symplectites may therefore represent the crystallized remnants of small melt fractions trapped within a deforming lithospheric mantle.

Following mylonitic deformation, continued exhumation led to progressive cooling of the mantle section and transition to brittle deformation. As temperatures declined, fluid infiltration became increasingly important, ultimately promoting widespread serpentinization. The onset of hydration is recorded by the development of tremolitic amphibole and minor hornblende (Table S2).

The scarcity of amphibole combined with the widespread development of serpentine indicates that hydration was ultimately dominated by pervasive serpentinization at temperatures <400°C (e.g., Alt & Shanks, 2003; Schwarzenbach et al., 2012), with amphibole representing a spatially limited retrograde phase. This suggests that amphibole formation was an early response to limited fluid infiltration, subsequently overprinted by extensive serpentinization during continued exhumation and cooling. The predominance of tremolite over hornblende suggests that the main phase of hydration took place at temperatures <500°C, with only localized amphibole growth at slightly higher temperatures (~600–650°C) for hornblende.

15252027, 2026, 10, Downloaded from https://agupubs.onlinelibrary.wiley.com/doi/10.1029/2026GC013203 by CochraneItalia, Wiley Online Library on [07/10/2026]. See the Terms and Conditions (https://onlinelibrary.wiley.com/terms-and-conditions) on Wiley Online Library for rules of use; OA articles are governed by the applicable Creative Commons License

6. Conclusions

The Newfoundland peridotites represent a fragment of subcontinental mantle exhumed during Triassic rifting in a magma-poor setting. Despite pervasive serpentinization, they preserve clear evidence of a multistage evolution predating rifting. High degrees of partial melting initiated in the garnet stability field, produced a strongly refractory mantle, subsequently overprinted by limited interaction with enriched melts. During rifting and breakup, this mantle section was reactivated within lithospheric-scale shear zones, where deformation, limited melt production, and local melt freezing likely accompanied mantle exhumation and mylonitization.

Comparison with the conjugate WIM suggests that inherited mantle features played a key role in controlling melt extraction, strain localization, and margin architecture. These results indicate that continental breakup is not solely governed by syn-rift processes but is strongly influenced by the long-term evolution and inherited characteristics of the lithospheric mantle.

Conflict of Interest

The authors declare no conflicts of interest relevant to this study.

Availability Statement

All data supporting the findings of this study are included in Supporting Information S1. They are also available in Zenodo via Secchiari, A. et al. (2026).

Acknowledgments
We thank O. Bruguier (Géosciences Montpellier) for LA-ICP-MS support, A. Risplendente for EMPA assistance at Unitech COSPECT (University of Milan), and A. Comelli for thin-section preparation. Professor Paul D. Asimow is gratefully acknowledged for his editorial handling. This paper benefited from the comments of I. Nishio and an anonymous reviewer, who significantly improved the initial version of this manuscript. This research was funded through MUR for ECORD-IODP Italia (Grant 9362021 awarded to A. Secchiari). This work has also benefited from the equipment and framework of the COMP-HUB and COMP-R initiatives funded by the "Departments of Excellence" program of the Italian Ministry for University and Research (MIUR 2018–2022; MUR 2023–2027). The authors also acknowledge the support of the APC central fund of the University of Milano as part of the Wiley - CRUI-CARE agreement. Open access publishing facilitated by Universita degli Studi di Milano, as part of the Wiley - CRUI-CARE agreement.

References

Abe, N. (2001). Petrochemistry of serpentinized peridotite from the Iberia Abyssal Plain (ODP Leg 173): Its character intermediate between sub-oceanic and sub-continental upper mantle. *Geological Society Special Publication*, *187*(1), 143–159. https://doi.org/10.1144/GSL.SP.2001.187.01.08

Alt, J. C., & Shanks, W. C. (2003). Serpentinization of abyssal peridotites from the MARK area, Mid-Atlantic Ridge: Sulfur geochemistry and reaction modeling. *Geochimica et Cosmochimica Acta*, *67*(4), 641–653. https://doi.org/10.1016/s0016-7037(02)01142-0

Barrett, N., Jaques, A. L., González-Álvarez, I., Walter, M. J., & Pearson, D. G. (2022). Ultra-refractory peridotites of Phanerozoic mantle origin: The Papua New Guinea ophiolite mantle tectonites. *Journal of Petrology*, *63*(3), egac014. https://doi.org/10.1093/PETROLOGY/EGAC014

Beard, J. S., Fullagar, P. D., & Sinha, A. K. (2002). Gabbroic pegmatite intrusions, Iberia Abyssal Plain, ODP Leg 173, Site 1070: Magmatism during a Transition from non-volcanic rifting to sea-floor spreading. *Journal of Petrology*, *43*(5), 885–905.

Birner, S. K., Warren, J. M., Cottrell, E., Davis, F. A., Kelley, K. A., & Falloon, T. J. (2017). Forearc peridotites from Tonga record heterogeneous oxidation of the mantle following subduction initiation. *Journal of Petrology*, *58*(9), 1755–1780. https://doi.org/10.1093/PETROLOGY/EGX072

Boillot, G., Recq, M., Winterer, E. L., Meyer, A. W., Applegate, J., Baltuck, M., et al. (1987). Tectonic denudation of the upper mantle along passive margins: A model based on drilling results (ODP leg 103, western Galicia margin, Spain). *Tectonophysics*, *132*(4), 335–342. https://doi.org/10.1016/0040-1951(87)90352-0

Brey, G. P., & Köhler, T. (1990). Geothermobarometry in four-phase lherzolites II. New thermobarometers, and practical assessment of existing thermobarometers. *Journal of Petrology*, *31*(6), 1353–1378. https://doi.org/10.1093/petrology/31.6.1353

Brunelli, D., Seyler, M., Cipriani, A., Ottolini, L., & Bonatti, E. (2006). Discontinuous melt extraction and weak refertilization of mantle peridotites at the Vema lithospheric section (Mid-Atlantic Ridge). *Journal of Petrology*, *47*(4), 745–771. https://doi.org/10.1093/PETROLOGY/EGI092

Chazot, G., Charpentier, S., Kornprobst, J., Vannucci, R., & Luais, B. (2005). Lithospheric mantle evolution during continental break-up: The West Iberia non-volcanic passive margin. *Journal of Petrology*, *46*(12), 2527–2568. https://doi.org/10.1093/petrology/egi064

Cluzel, D., Ulrich, M., Jourdan, F., Meffre, S., Paquette, J. L., Audet, M. A., et al. (2016). Early Eocene clinoenstatite boninite and boninite-series dikes of the ophiolite of New Caledonia; a witness of slab-derived enrichment of the mantle wedge in a nascent volcanic arc. *Lithos*, *260*, 429–442. https://doi.org/10.1016/j.lithos.2016.04.031

Cornen, G., Beslier, M.-O., & Girardeau, J. (1996). Petrologic characteristics of the ultramafic rocks from the ocean/continent transition in the Iberia Abyssal Plain. In *Proceedings of the Ocean Drilling Program, Scientific Results* (Vol. 149, pp. 377–395).

Cornen, G., Beslier, M.-O., & Girardeau, J. (1996). Petrology of the mafic rocks cored in the Iberia Abyssal Plain. In *Proceedings of the Ocean Drilling Program Scientific Results* (Vol. 149, pp. 449–470). https://doi.org/10.2973/ODP.PROC.SR.149.220.1996

D'Errico, M. E., Warren, J. M., & Godard, M. (2016). Evidence for chemically heterogeneous Arctic mantle beneath the Gakkel Ridge. *Geochimica et Cosmochimica Acta*, *174*, 291–312. https://doi.org/10.1016/j.gca.2015.11.017

Dick, H. J. B., & Bullen, T. (1984). Chromian spinel as a petrogenetic indicator in abyssal and alpine-type peridotites and spatially associated lavas. *Contributions to Mineralogy and Petrology*, *86*(1), 54–76. https://doi.org/10.1007/BF00373711

Dijkstra, A. H., Sergeev, D. S., Spandler, C., Pettke, T., Meisel, T., & Cawood, P. a. (2010). Highly refractory peridotites on Macquarie Island and the case for anciently depleted domains in the Earth's mantle. *Journal of Petrology*, *51*(1–2), 469–493. https://doi.org/10.1093/petrology/egp084

Downes, H. (2001). Formation and modification of the shallow sub-continental lithospheric mantle: A review of geochemical evidence from ultramatic xenolith suites and tectonically emplaced ultramafic massifs of Western and Central Europe. *Journal of Petrology*, *42*(1), 233–250. https://doi.org/10.1093/petrology/42.1.233

Downes, H., de Vries, C., & Wittig, N. (2015). Hf -Zr anomalies in clinopyroxene from mantle xenoliths from France and Poland: Implications for Lu- Hf dating of spinel peridotite lithospheric mantle. *International Journal of Earth Sciences*, *104*(1), 89–102. https://doi.org/10.1007/s00531-014-1074-x

Downes, H., Reichow, M. K., Mason, P. R. D., Beard, A. D., & Thirlwall, M. F. (2003). Mantle domains in the lithosphere beneath the French Massif Central:Trace element and isotopic evidence from mantle clinopyroxenes. *Chemical Geology*, *200*(1–2), 71–87. https://doi.org/10.1016/S0009-2541(03)00126-8

Godard, M., Bodinier, J. L., & Vasseur, G. (1995). Effects of mineralogical reactions on trace element redistributions in mantle rocks during percolation processes: A chromatographic approach. *Earth and Planetary Science Letters*, *133*(3–4), 449–461. https://doi.org/10.1016/0012-821X(95)00104-K

Harigane, Y., Michibayashi, K., Morishita, T., Tamura, A., Hashimoto, S., & Snow, J. E. (2022). Deformation beneath Gakkel Ridge, Arctic Ocean: From mantle flow to mantle shear in a sparsely magmatic spreading zone. *Tectonophysics*, *822*, 229186. https://doi.org/10.1016/J.TECTO.2021.229186

Hart, S. R., & Dunn, T. (1993). Experimental Cpx/Melt partitioning of 24 trace elements. *Contributions to Mineralogy and Petrology*, *113*, 1–8. https://doi.org/10.1007/bf00320827

Hébert, R., Gueddari, K., Laflèche, M. R., Beslier, M. O., & Gardien, V. (2001). Petrology and geochemistry of exhumed peridotites and gabbros at non-volcanic margins: ODP Leg 173 West Iberia ocean-continent transition zone. *Geological Society Special Publication*, *187*(1), 161–189. https://doi.org/10.1144/GSL.SP.2001.187.01.09

Hellebrand, E., Snow, J. E., Dick, H. J., & Hofmann, a. W. (2001). Coupled major and trace elements as indicators of the extent of melting in mid-ocean-ridge peridotites. *Nature*, *410*(6829), 677–681. https://doi.org/10.1038/35070546

Hellebrand, E., Snow, J. E., Hoppe, P., & Hofmann, A. W. (2002). Garnet-field melting and late-stage refertilization in "residual" abyssal peridotites from the Central Indian Ridge. *Journal of Petrology*, *43*(12), 2305–2338. https://doi.org/10.1093/petrology/43.12.2305

Holtzman, B. K., Kohlstedt, D. L., Zimmerman, M. E., Heidelbach, F., Hiraga, T., & Hustoft, J. (2003). Melt segregation and strain partitioning: Implications for seismic anisotropy and mantle flow. *Science*, *301*(5637), 1227–1230. https://doi.org/10.1126/science.1087132

Ionov, D. A., Bodinier, J. L., Mukasa, S. B., & Zanetti, A. (2002). Mechanisms and sources of mantle metasomatism: Major and trace element compositions of peridotite xenoliths from Spitsbergen in the context of numerical modelling. *Journal of Petrology*, *43*(12), 2219–2259. https://doi.org/10.1093/petrology/43.12.2219

Ishii, T., Robinson, P. T., Maekawa, H., & Fiske, R. (1992). Petrological studies of peridotites from diapiric serpentinite seamounts in the Izu-Ogasawara-Mariana Forearc, Leg 125. *Proceedings of the Ocean Drilling Program, Scientific Results*, *125*, 445–485. https://doi.org/10.2973/odp.proc.sr.125.129.1992

Jagoutz, O., Müntener, O., Manatschal, G., Rubatto, D., Péron-Pinvidic, G., Turrin, B. D., & Villa, I. M. (2007). The rift-to-drift transition in the North Altantic: A stuttering start of the MORB machine? *Geology*, *35*(12), 1087–1090. https://doi.org/10.1130/G23613A.1

Jochum, K. P., Stoll, B., Herwig, K., Willbold, M., Hofmann, A. W., Amini, M., et al. (2005). MPI-DING reference glasses for in situ micro-analysis: New reference values for element concentrations and isotope ratios. *Geochemistry, Geophysics, Geosystems*, *7*(2), Q02008. https://doi.org/10.1029/2005gc001060

Kaczmarek, M. A., & Müntener, O. (2008). Juxtaposition of melt impregnation and high-temperature shear zones in the upper mantle; field and petrological constraints from the Lanzo Peridotite (Northern Italy). *Journal of Petrology*, *49*(12), 2187–2220. https://doi.org/10.1093/petrology/egn065

Katz, R. F., Spiegelman, M., & Holtzman, B. (2006). The dynamics of melt and shear localization in partially molten aggregates. *Nature*, *442*(7103), 676–679. https://doi.org/10.1038/nature05039

Kodolányi, J., Pettke, T., Spandler, C., Kamber, B. S., & Gméling, K. (2012). Geochemistry of ocean floor and fore-arc serpentinites: Constraints on the ultramafic input to subduction zones. *Journal of Petrology*, *53*(2), 235–270. https://doi.org/10.1093/petrology/egr058

Kornprobst, J., & Tabit, A. (1988). 7. Plagioclase-bearing ultramafic tectonites from the Galicia margin (leg 103, site 637): Comparison of their origin and evolution with low-pressure ultramafic bodies in western Europe. In *Proceedings of the Ocean Drilling Program, Scientific Results* (Vol. 103).

Leake, B. E., Woolley, A. R., Arps, C. E. S., Birch, W. D., Gilbert, M. C., Grice, J. D., et al. (1997). Nomenclature of amphiboles; report of the subcommittee on amphiboles of the International Mineralogical Association Commission on New Minerals and Mineral Names. *Mineralogical Magazine*, *61*(405), 295–310. https://doi.org/10.1180/MINMAG.1997.061.405.13

Liang, Y., Sun, C., & Yao, L. (2013). A REE-in-two-pyroxene thermometer for mafic and ultramafic rocks. *Geochimica et Cosmochimica Acta*, *102*, 246–260. https://doi.org/10.1016/j.gca.2012.10.035

Lindsley, D. H. (1983). Pyroxene thermometry. *American Mineralogist*, *68*(5–6), 477–493.

Lymer, G., & Reston, T. J. (2022). The west Iberian margin: Past and current research concepts and future challenges. Retrieved from www.iste.co.uk/peronpinvidic/

Morishita, T., & Arai, S. (2003). Evolution of spinel–pyroxene symplectite in spinel–lherzolites from the Horoman Complex, Japan. *Contributions to Mineralogy and Petrology*, *144*(5), 509–522. https://doi.org/10.1007/s00410-002-0417-y

Müntener, O., & Manatschal, G. (2006). High degrees of melt extraction recorded by spinel harzburgite of the Newfoundland margin: The role of inheritance and consequences for the evolution of the southern North Atlantic. *Earth and Planetary Science Letters*, *252*(3–4), 437–452. https://doi.org/10.1016/j.epsl.2006.10.009

Nishio, I., Akizawa, N., Ishii, T., Itano, K., Tamura, A., & Morishita, T. (2026). Residual forearc peridotites recording the early magmatic stage of subduction initiation. *Geochemical Perspectives Letters*, *41*, 1–6. https://doi.org/10.7185/geochemlet.2624

Niu, Y. (2004). Bulk-rock major and trace element compositions of abyssal peridotites: Implications for mantle melting, melt extraction and post-melting processes beneath mid-ocean ridges. *Journal of Petrology*, *45*(12), 2423–2458. https://doi.org/10.1093/petrology/egh068

Norman, M. D. (1998). Melting and metasomatism in the continental lithosphere: Laser ablation ICPMS analysis of minerals in spinel lherzolites from Eastern Australia. *Contributions to Mineralogy and Petrology*, *130*(3–4), 240–255. https://doi.org/10.1007/s004100050363

Parkinson, I. J., & Pearce, J. A. (1998). Peridotites from the Izu-Bonin-Mariana forearc (ODP leg 125): Evidence for mantle melting and melt-mantle interaction in a supra-subduction zone setting. *Journal of Petrology*, *39*(9), 1577–1618. https://doi.org/10.1093/petroj/39.9.1577

Pearce, N. J., Perkins, W. T., Westgate, J. A., Gorton, M. P., Jackson, S. E., Neal, C. R., & Chenery, S. P. (1997). A compilation of new and published major and trace element data for NIST SRM 610 and NIST SRM 612 glass reference materials. *Geostandards Newsletter*, *21*(1), 115–144. https://doi.org/10.1111/j.1751-908x.1997.tb00538.x

Péron-Pinvidic, G., & Manatschal, G. (2009). The final rifting evolution at deep magma-poor passive margins from Iberia-Newfoundland: A new point of view. *International Journal of Earth Sciences*, *98*(7), 1581–1597. https://doi.org/10.1007/s00531-008-0337-9

Péron-Pinvidic, G., Manatschal, G., Minshull, T. A., & Sawyer, D. S. (2007). Tectonosedimentary evolution of the deep Iberia-Newfoundland margins: Evidence for a complex breakup history. *Tectonics*, *26*(2). https://doi.org/10.1029/2006TC001970

15252027, 2026, 10, Downloaded from https://agupubs.onlinelibrary.wiley.com/doi/10.1029/2026GC013203 by CochraneItalia, Wiley Online Library on [07/10/2026]. See the Terms and Conditions (https://onlinelibrary.wiley.com/terms-and-conditions) on Wiley Online Library for rules of use; OA articles are governed by the applicable Creative Commons License

Picazo, S., Lafay, R., Faucheux, V., & Vennemann, T. (2019). New constraints on carbonation associated with brecciation in hyperextended margins (example of Iberia and Newfoundland margins). *Terra Nova*, *31*(4), 317–331. https://doi.org/10.1111/ter.12383

Rampone, E., Bottazzi, P., & Ottolini, L. (1991). Complementary Ti and Zr anomalies in orthopyroxene and clinopyroxene from mantle peridotites. *Nature*, *354*(6354), 518–520. https://doi.org/10.1038/354518a0

Rampone, E., Vissers, R. L. M., Poggio, M., Scambelluri, M., & Zanetti, A. (2009). Melt migration and intrusion during exhumation of the Alboran lithosphere: The Tallante mantle xenolith record (Betic Cordillera, SE Spain). *Journal of Petrology*, *51*(1–2), 295–325. https://doi.org/10.1093/petrology/egp061

Salters, V. J. M., & Stracke, A. (2004). Composition of the depleted mantle. *Geochemistry, Geophysics, Geosystems*, *5*(5), Q05B07. https://doi.org/10.1029/2003gc000597

Schwarzenbach, E., Früh-Green, G. L., Bernasconi, S. M., Alt, J. C., Shanks, W. C., Gaggero, L., & Crispini, L. (2012). Sulfur geochemistry of peridotite-hosted hydrothermal systems: Comparing the Ligurian ophiolites with oceanic serpentinites. *Geochimica et Cosmochimica Acta*, *91*, 283–305. https://doi.org/10.1016/j.gca.2012.05.021

Scott, J. M., Hodgkinson, A., Palin, J. M., Waight, T. E., Van der Meer, Q. H. A., & Cooper, A. F. (2014). Ancient melt depletion overprinted by young carbonatitic metasomatism in the New Zealand lithospheric mantle. *Contributions to Mineralogy and Petrology*, *167*(1), 1–17. https://doi.org/10.1007/s00410-014-0963-0

Scott, J. M., Liu, J., Pearson, D. G., & Waight, T. E. (2016). Mantle depletion and metasomatism recorded in orthopyroxene in highly depleted peridotites. *Chemical Geology*, *441*, 280–291. https://doi.org/10.1016/J.CHEMGEO.2016.08.024

Secchiari, A., Godard, M., & Montanini, A. (2025). Mantle heterogeneity generated by melt depletion and melt–rock interaction: The West Iberian margin peridotites (ODP Leg 149 and 173). *Journal of Petrology*, *66*(2), egaf005. https://doi.org/10.1093/petrology/egaf005

Secchiari, A., Godard, M., & Montanini, A. (2026). Dataset for the paper "Multistage Evolution and Inheritance in a Magma-Poor Conjugate Margin: Insights from Serpentinized Peridotites of the Newfoundland Margin (ODP Hole 1277A)" [Dataset]. In *Geochemistry, Geophysics, Geosystems*. Zenodo. https://doi.org/10.5281/zenodo.22232462

Secchiari, A., Montanini, A., Bosch, D., Macera, P., & Cluzel, D. (2020). Sr, Nd, Pb and trace element systematics of the New Caledonia harzburgites: Tracking source depletion and contamination processes in a SSZ setting. *Geoscience Frontiers*, *11*(1), 37–55. https://doi.org/10.1016/j.gsf.2019.04.004

Seifert, K. E., Chang, C.-W., & Brunotte, D. A. (1997). Evidence from Ocean Drilling Program Leg 149 mafic igneous rocks for oceanic crust in the Iberia Abyssal Plain ocean-continent transition zone. *Journal of Geophysical Research*, *102*(B4), 7915–7928. https://doi.org/10.1029/96jb03912

Seyler, M., Brunelli, D., Toplis, M. J., & Mével, C. (2011). Multi-scale chemical heterogeneities beneath the eastern Southwest Indian Ridge (52°E–68°E): Trace element compositions of along-axis dredged peridotites. *Geochemistry, Geophysics, Geosystems*, *12*(9), Q0AC15. https://doi.org/10.1029/2011GC003585

Seyler, M., Lorand, J.-P., Dick, H. J. B., & Drouin, M. (2007). Pervasive melt percolation reactions in ultra-depleted refractory harzburgites at the Mid-Atlantic Ridge, 15° 20′N: ODP Hole 1274A. *Contributions to Mineralogy and Petrology*, *153*(3), 303–319. https://doi.org/10.1007/s00410-006-0148-6

Seyler, M., Toplis, M. J., Lorand, J. P., Luguet, a., & Cannat, M. (2001). Clinopyroxene microtextures reveal incompletely extracted melts in abyssal peridotites. *Geology*, *29*(2), 155–158. https://doi.org/10.1130/0091-7613(2001)029<0155:CMRIEM>2.0.CO

Shervais, J. W., & Jean, M. M. (2012). Inside the subduction factory: Modeling fluid mobile element enrichment in the mantle wedge above a subduction zone. *Geochimica et Cosmochimica Acta*, *95*, 270–285. https://doi.org/10.1016/J.GCA.2012.07.006

Shervais, J. W., Reagan, M. K., Godard, M., Prytulak, J., Ryan, J. G., Pearce, J. A., et al. (2021). Magmatic response to subduction initiation, Part II: Boninites and related rocks of the Izu-Bonin Arc from IODP Expedition 352. *Geochemistry, Geophysics, Geosystems*, *22*(1), e2020GC009093. https://doi.org/10.1029/2020GC009093

Shillington, D. J., Holbrook, W. S., Van Avendonk, H. J. A., Tucholke, B. E., Hopper, J. R., Louden, K. E., et al. (2006). Evidence for asymmetric nonvolcanic rifting and slow incipient oceanic accretion from seismic reflection data of the Newfoudland margin. *Journal of Geophysical Research*, *111*(9), B09402. https://doi.org/10.1029/2005JB003981

Shimizu, Y., Arai, S., Morishita, T., & Ishida, Y. (2008). Origin and significance of spinel–pyroxene symplectite in lherzolite xenoliths from Tallante, SE Spain. *Mineralogy and Petrology*, *94*(1–2), 27–43. https://doi.org/10.1007/s00710-008-0004-7

Suhr, G., Kelemen, P., & Paulick, H. (2008). Microstructures in Hole 1274A peridotites, ODP Leg 209, Mid-Atlantic Ridge: Tracking the fate of melts percolating in peridotite as the lithosphere is intercepted. *Geochemistry, Geophysics, Geosystems*, *9*(3), Q03012. https://doi.org/10.1029/2007GC001726

Sun, S.-S., & McDonough, W. F. (1989). Chemical and isotopic systematics of oceanic basalts: Implications for mantle composition and processes. *Geological Society, London, Special Publications*, *42*(1), 313–345. https://doi.org/10.1144/GSL.SP.1989.042.01.19

Takahashi, N. (2001). Origin of plagioclase Lherzolite from the Nikanbetsu peridotite complex, Hokkaido, northern Japan: Implications for incipient melt migration and segregation in the partially molten upper mantle. *Journal of Petrology*, *42*(1), 39–54. https://doi.org/10.1093/petrology/42.1.39

Tucholke, B., Sawyer, D., & Sibuet, J. (2007). Breakup of the Newfoundland Iberia rift. *Geological Society London Special Publications*, *282*(1), 9–46. https://doi.org/10.1144/sp282.2

Tucholke, B. E., & Sibuet, J.-C. (2007). Leg 210 Synthesis: Tectonic, magmatic, and sedimentary evolution of the Newfoundland-Iberia rift. *Proceedings of the Ocean Drilling Program, Scientific Results*, *210*, 1–56. https://doi.org/10.2973/odp.proc.sr.210.101.2007

van Achterberg, E., Ryan, C. G., & Griffin, W. L. (2001). *GLITTER user's manual: On-line interactive data reduction for the LA-ICP-MS mieroprobe. Version 4*. North Ryde: Maequarie Research Limited.

Vernières, J., Godard, M., & Bodinier, J.-L. (1997). A plate model for the simulation of trace element fractionation during partial melting and magma transport in the Earth's upper mantle. *Journal of Geophysical Research*, *102*(B11), 24771–24784. https://doi.org/10.1029/97JB01946

Vesin, C., Rubatto, D., Pettke, T., & Deloule, E. (2023). Multistage hydration during oceanic serpentinisation revealed by in situ oxygen isotope and trace element analyses. *Geochimica et Cosmochimica Acta*, *355*, 13–31. https://doi.org/10.1016/j.gca.2023.06.032

Walter, M. J. (1998). Melting of garnet peridotite and the origin of komatiite and depleted lithosphere. *Journal of Petrology*, *39*(1), 29–60. https://doi.org/10.1093/petroj/39.1.29

Warren, J. M. (2016). Global variations in abyssal peridotite compositions. *Lithos*, *248–251*, 193–219. https://doi.org/10.1016/j.lithos.2015.12.023

Welford, J. K. (2025). Unusually fracture-free seafloor in the southern North Atlantic between Newfoundland and Iberia explained through compounding tectonic inheritance since the Paleoproterozoic. *Geology*, *53*(6), 483–487. https://doi.org/10.1130/G53057.1

15252027, 2026, 10, Downloaded from https://agupubs.onlinelibrary.wiley.com/doi/10.1029/2026GC013203 by CochraneItalia, Wiley Online Library on [07/10/2026]. See the Terms and Conditions (https://onlinelibrary.wiley.com/terms-and-conditions) on Wiley Online Library for rules of use; OA articles are governed by the applicable Creative Commons License

Whitmarsh, R. B., & Sawyer, D. S. (1996). The ocean/continent transition beneath the Iberia Abyssal Plain and continental-rifting to seafloor-spreading processes. In *Proceedings of the Ocean Drilling Program Scientific Results* (Vol. 149, pp. 713–733). https://doi.org/10.2973/odp.proc.sr.149.249.1996

Witt-Eickschen, G., & Kramm, U. (1997). Mantle upwelling and metasomatism beneath central Europe: Geochemical and isotopic constraints from Mantle xenoliths from the Rhön (Germany). *Journal of Petrology*, *38*.

Xu, X., O'Reilly, S. Y., Griffin, W. L., & Zhou, X. (2000). Genesis of young lithospheric mantle in Southeastern China: An LAM-ICPMS trace element study. *Journal of Petrology*, *41*(1), 111–148. https://doi.org/10.1093/petrology/41.1.111

15252027, 2026, 10, Downloaded from https://agupubs.onlinelibrary.wiley.com/doi/10.1029/2026GC013203 by CochraneItalia, Wiley Online Library on [07/10/2026]. See the Terms and Conditions (https://onlinelibrary.wiley.com/terms-and-conditions) on Wiley Online Library for rules of use; OA articles are governed by the applicable Creative Commons License